A Genome-Scale Metabolic Model of Soybean (*Glycine max*) Highlights Metabolic Fluxes in Seedlings[1][OPEN]

Thiago Batista Moreira,[a] Rahul Shaw,[b] Xinyu Luo,[b] Oishik Ganguly,[b] Hyung-Seok Kim,[b] Lucas Gabriel Ferreira Coelho,[a] Chun Yue Maurice Cheung,[b,2] and Thomas Christopher Rhys Williams[a,2,3]

[a]Departament of Botany, University of Brasília, Campus Darcy Ribeiro, Asa Norte, Brasília, Brazil, 70910-900
[b]Division of Science, Yale-National University of Singapore College, Singapore, 138527

ORCID IDs: 0000-0001-5074-9544 (T.B.M.); 0000-0002-5154-1427 (R.S.); 0000-0003-0521-4975 (O.G.); 0000-0003-1649-6218 (L.G.F.C.); 0000-0002-5531-7895 (C.Y.M.C.); 0000-0003-1954-2961 (T.C.R.W.).

Until they become photoautotrophic juvenile plants, seedlings depend upon the reserves stored in seed tissues. These reserves must be mobilized and metabolized, and their breakdown products must be distributed to the different organs of the growing seedling. Here, we investigated the mobilization of soybean (*Glycine max*) seed reserves during seedling growth by initially constructing a genome-scale stoichiometric model for this important crop plant and then adapting the model to reflect metabolism in the cotyledons and hypocotyl/root axis (HRA). A detailed analysis of seedling growth and alterations in biomass composition was performed over 4 d of postgerminative growth and used to constrain the stoichiometric model. Flux balance analysis revealed marked differences in metabolism between the two organs, together with shifts in primary metabolism occurring during different periods postgermination. In particular, from 48 h onward, cotyledons were characterized by the oxidation of fatty acids to supply carbon for the tricarboxylic acid cycle as well as production of sucrose and glutamate for export to the HRA, while the HRA was characterized by the use of a range of imported amino acids in protein synthesis and catabolic processes. Overall, the use of flux balance modeling provided new insight into well-characterized metabolic processes in an important crop plant due to their analysis within the context of a metabolic network and reinforces the relevance of the application of this technique to the analysis of complex plant metabolic systems.

During germination and the postgerminative growth that follows emergence of the radicle from the testa, plants depend on reserves previously accumulated in the embryonic axis, cotyledons, or endosperm of the seed (Buckeridge et al., 2004; Castro et al., 2004; Finch-Savage and Leubner-Metzger, 2006). Mobilization of such reserves, including proteins, lipids, and carbohydrates, supplies the carbon- and nitrogen-containing precursors necessary for the production of new seedling biomass as well as the ATP and reducing equivalents required for tissue growth and maintenance (Ziegler, 1995; Buckeridge et al., 2004). The quantity and quality of these reserves exhibit significant variation between species but are also affected by environmental conditions experienced by the mother plant during seed development (Spears et al., 1997; Rotundo and Westgate, 2009).

Due to the critical role that they play in germination and seedling growth, the metabolic pathways responsible for reserve mobilization have received a lot of attention. Carbohydrates, such as Suc, raffinose series oligosaccharides (RFOs), starch, and cell wall polysaccharides, are broken down, and the resulting carbon skeletons are fed into glycolysis and the pentose phosphate pathway or used in the production of new starch and cell walls (Buckeridge et al., 1995; Buckeridge and Dietrich, 1996; Gronwald et al., 2009). Triacylglycerol is hydrolyzed to release fatty acids that are in turn broken down via β-oxidation to produce acetyl-CoA (Graham, 2008), which may then be used via the glyoxylate cycle and gluconeogenesis in the production of sugars or to support respiration (Eastmond and Graham, 2001; Eastmond et al., 2015). Protein is also hydrolyzed, releasing its constituent amino acids (Tan-Wilson and Wilson, 2012), which may be used directly in the production of new protein or may be degraded and the breakdown products fed into other pathways (Hildebrandt et al., 2015).

Crucially, though, these processes act not in isolation but within the context of a metabolic network (Kruger and Ratcliffe, 2015), as intermediates of such degradative pathways also participate as substrates and products of

[1]This work was supported by the Brazilian organizations FINATEC (travel grant 2015), Ministry of Science, Technology, and Innovation, Conselho Nacional de Desenvolvimento Cientfico e Tecnolgico (universal grant 483870/2013-7), FINEP (CT-INFRA program), and the Coordenação de Aperfeiçoamento de Pessoal de Nível Superior (Finance Code 001).

[2]Senior authors.

[3]Author for contact: tcrwilliams@unb.br.

The author responsible for distribution of materials integral to the findings presented in this article in accordance with the policy described in the Instructions for Authors (www.plantphysiol.org) is: Thomas Christopher Rhys Williams (tcrwilliams@unb.br).

T.B.M. and L.G.F.C. designed and performed the experiments; R.S., O.G., X.L., H.-S.K., and C.Y.M.C. built and tested the genome-scale model; R.S. and C.Y.M.C. carried out the simulations; T.C.R.W., T.B.M., and C.Y.M.C. conceived the project, analyzed the data, and wrote the article; T.C.R.W. supervised the project.

[OPEN]Articles can be viewed without a subscription.

www.plantphysiol.org/cgi/doi/10.1104/pp.19.00122

many other reactions, and the breakdown of different reserves is therefore interconnected. Furthermore, different metabolic processes act in concert to meet the cellular demand for the ATP and reducing equivalents that are required to assemble metabolic precursors into components of biomass and maintain plant cell functions. While we currently have a good idea of the individual processes that act during reserve mobilization, the manner in which these processes interact to meet the carbon, nitrogen, and energy demands of a growing seedling has received less attention.

This is particularly relevant when considering seeds that contain a mixture of different reserves and where the degradation of some, or all, of these reserves occurs simultaneously. Soybean (*Glycine max*) contains large quantities of proteins, lipids, and carbohydrates, which has led to its extensive use as a source of animal feed and biodiesel as well as in human nutrition (Chaudhary et al., 2015), uses that in turn are responsible for the large-scale planting of this crop and the production of more than 361 million tons of soybeans worldwide in 2018 (www.soystats.com). Soybeans typically contain between 40% and 45% of dry mass as protein, with 70% to 80% of this protein in the form of the reserve proteins glycinin and β-conglycinin (Nielsen, 1996). Oil makes up an average of 20% of the dry weight (Clemente and Cahoon, 2009), with the majority in the form of triacylglycerol-containing monounsaturated and polyunsaturated fatty acids (Morais and Silva, 1996; Clemente and Cahoon, 2009). Finally, soybeans also contain between 20% and 35% of dry mass as carbohydrates (Morais and Silva, 1996). This carbohydrate exists principally in the form of Suc (41%–68%) and the RFO stachyose (12%–35%) and raffinose (5%–16%; Nielsen, 1996), with starch representing only 1% to 3% of the total dry mass (Yazdi-Samadi et al., 1977). While specific reserves and metabolic processes are considered more important during certain phases of seed germination and postgerminative growth (Weitbrecht et al., 2011), we lack information regarding the relative contributions of different reserves in carbon, nitrogen, and energy balance during different developmental phases, in part because the computational tools required to obtain such information have only recently become available.

Metabolic modeling of seedling reserve mobilization and metabolism is necessary if we are to fully understand these processes. Among the frameworks available for the construction and analysis of metabolic models, flux balance analysis (FBA) using genome-scale models stands out due to its capacity to cover entire metabolic networks. Indeed, FBA has been applied extensively to the analysis of bacterial, yeast, animal, and plant metabolism (Kruger and Ratcliffe, 2015; Nikoloski et al., 2015; Moreira et al., 2019). Recent studies in plants have extended the use of FBA to diel cycles (Cheung et al., 2014), different cell types in C4 photosynthesis (Dal'Molin et al., 2010), the development of tomato (*Solanum lycopersicum*) fruit (Colombié et al., 2015), different organs within developing seeds (Rolletschek et al., 2015), interactions between nodule bacteroids and the model legume *Medicago truncatula* (Pfau et al., 2018), and even entire plants (Grafahrend-Belau et al., 2013; Dal'Molin et al., 2015; Shaw and Cheung, 2018). Studies of this nature have generated important insight into the operation of plant primary metabolism as well as the relationship between sources and sink organs, making FBA particularly useful to the study of seed reserve mobilization. In this study, we constructed a genome-scale metabolic model of soybean and used FBA to explore reserve mobilization in this important crop during postgerminative growth, defined as the period following radicle protrusion from the testa (Bewley, 1997; Finch-Savage and Leubner-Metzger, 2006), with the aim of identifying how the different seed reserves and metabolic processes meet the demands of the growing seedling. Such information, in addition to increasing our understanding of the roles of different seed reserves, may be used in the future to rationalize the effects of alterations in seed composition on seedling growth and establishment as well as to suggest potential targets for engineering of seedling metabolism (Libourel and Shachar-Hill, 2008; Simeonidis and Price, 2015).

RESULTS

A Genome-Scale Metabolic Model of Soybean and Its General Properties

In order to study reserve mobilization and metabolism during seedling growth, we constructed a genome-scale metabolic model of soybean (Supplemental File S1). The model was constructed based on SoyCyc version 6.0 (http://plantcyc.org/databases/soycyc/6.0) and represents a mass and charge balanced metabolic network of soybean that is capable of phototrophic and heterotrophic production of all biomass components. Other than the major biomass precursors of carbohydrates, proteins, lipids, lignin, and nucleotides, the model also includes several biomass components for monosaccharides, disaccharides, and oligosaccharides, glycosides, alcohols, chlorophyll, etc., to represent the biosynthesis and hydrolysis of biopolymers and noncentral metabolic activities. Reactions related to the remobilization of seed reserves were also included to allow modeling of metabolic activity during seedling growth.

The soybean genome-scale metabolic model contains 2,814 metabolites and 3,001 reactions, of which 1,798 reactions are associated with 6,127 unique genes. Among the 3,001 reactions, there are 109 reactions for the synthesis of biomass components, 17 reactions representing exchange of metabolites with the environment, and 227 intracellular metabolite transporters. Model construction, curation, and testing are described in detail in "Materials and Methods."

The curated and tested metabolic model was used to construct a multiorgan model that represents the cotyledons and hypocotyl/root axis (HRA) of soybean seedlings (Supplemental File S2). Figure 1A shows the schematic description of the multiorgan model, including metabolite exchanges between cotyledons and HRA.

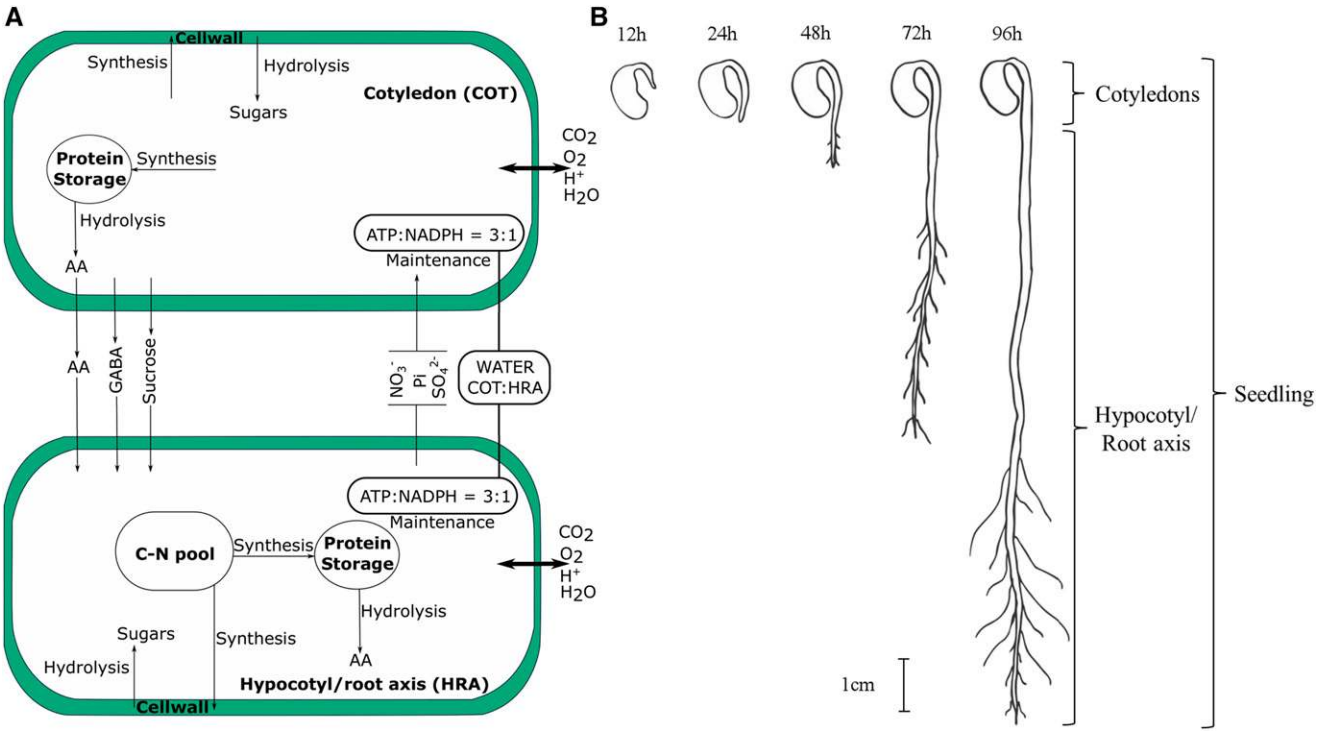

Figure 1. Schematic description of the multiorgan model representing soybean seedlings and the interaction between the cotyledon (COT) and HRA. Metabolite exchanges between the two organs are allowed through the phloem, which contained the 20 standard amino acids (AA), GABA, and Suc transporters. Cell wall and protein hydrolysis and degradation were present in both the organs. ATP:NADPH maintenance reactions allowed a ratio of 3:1 in an individual organ, and the maintenance ratio between organs is constrained using their water content as a proxy for metabolic activity. CO_2, oxygen, proton, and water were allowed free exchange with the environment.

In this study, the multiorgan model was used to study the metabolic activities of soybean seedlings during early postgerminative growth.

Growth and Biomass Composition of Soybean Seedlings

To understand the pattern of seed reserve mobilization and generate experimental constraints for use with the genome-scale multiorgan model, we analyzed the growth and composition of soybean seedlings during germination and postgerminative growth (Figs. 2 and 3). Soybean seeds germinated (defined as emergence of the radicle from the testa) at around 24 h after the beginning of imbibition and, following germination, HRA dry mass increased gradually throughout the rest of the experiment while the mass of each cotyledon pair decreased, reflecting the mobilization of reserves and their transport to the growing HRA (Fig. 2). Water content of the HRA increased dramatically between 12 and 48 h, indicating the significant uptake of water necessary to drive cell expansion and seedling growth (Fig. 1B; Supplemental Fig. S1).

Levels of carbon remained constant in the cotyledons during the experiment (54% of dry mass; Supplemental Fig. S2A), but the proportion of HRA biomass that was carbon decreased from 50% at 24 h to 40% at 72 h (Supplemental Fig. S2B), indicating a significant alteration in the composition of this organ. In cotyledons, nitrogen levels varied little (7%–7.5%; Supplemental Fig. S3A), while in the HRA, a significant decrease occurred between 12 and 72 h (7.2%–5.6%; Supplemental Fig. S3B). Total transesterifiable fatty acids remained

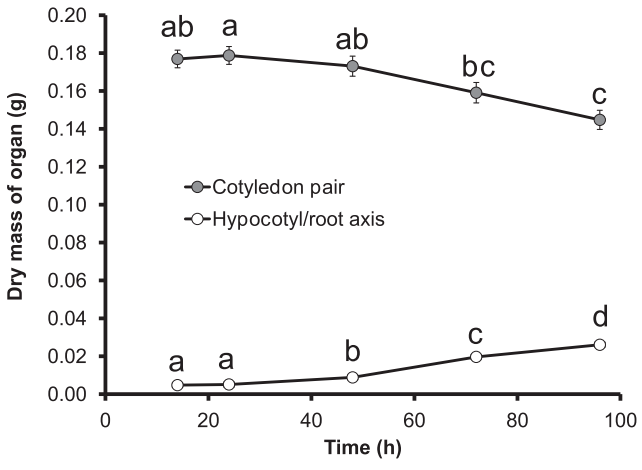

Figure 2. Changes in dry mass of cotyledon pairs and the HRA of soybean seedlings following imbibition. Values are means and SE of five groups of seedlings or 10 groups of seedlings for the 24-h time point. Different letters indicate significant differences between means (Tukey's test, $P < 0.05$)

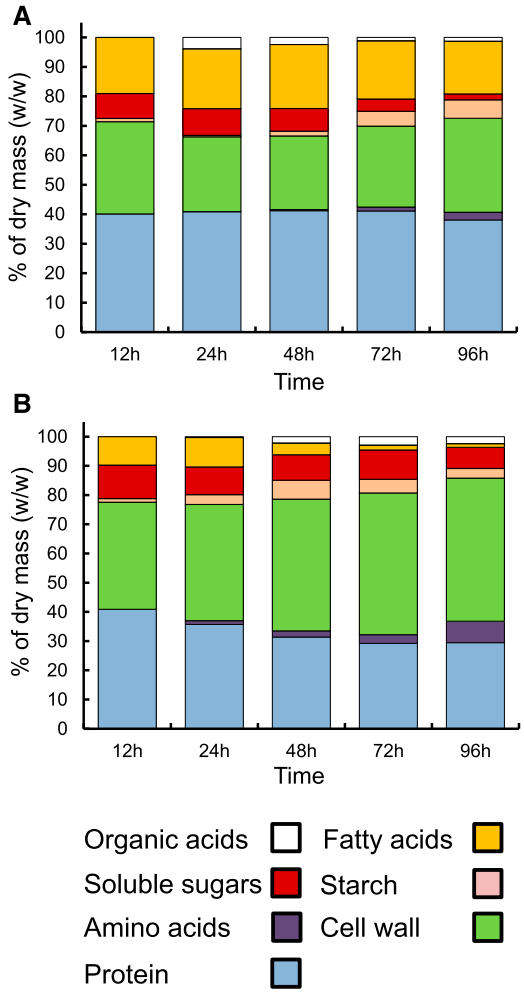

Figure 3. Composition of cotyledon and HRA biomass at different times following the beginning of imbibition. Data sources are described in the text and supplemental information (Supplemental Figs. S1–S8; Supplemental Tables S1–S5). Organic acids and free amino acids were not quantified at the 12-h time point.

relatively constant in cotyledons at around 20% of dry mass (Supplemental Fig. S4A), consistent with previously reported values for this variety (19.7% oil; Empresa Brasileira de Pesquisa Agropecuária, 1996), although we did detect a significant decrease in levels between 48 and 96 h. The most abundant fatty acids were linoleic acid (~60% of total fatty acids) and oleic acid (20%), with palmitic acid and linolenic acid making up 10% of fatty acids (Supplemental Table S1) with only slight changes occurring over the course of the experiment. Fatty acid levels in the HRA, on the other hand, decreased substantially after 24 h, from around 10% to 1% of dry mass at the end of the experiment (Supplemental Fig. S4B). Composition was similar to that observed in the cotyledons, although with a much lower level of oleic acid (2%) and a greater level of linolenic acid (around 30%; Supplemental Table S2).

Imbibed cotyledons contained high levels of Suc and stachyose (5.1% and 2.6% of dry mass, respectively) and lower levels of raffinose (0.7%; Supplemental Table S3). Total soluble sugars initially increased (Supplemental Fig. S5); however, from 24 h, we observed consumption of stachyose, with its almost total consumption by 96 h. Suc also decreased from 48 h onward, reaching 1.6% of dry mass at 96 h. The HRA also contained high levels of Suc (4% of dry mass) and stachyose (6.2%) at 12 h (Supplemental Table S4). RFOs were totally consumed by 48 h, while Suc levels increased to 5.9% by 24 h before decreasing to 0.7% at 96 h. Concomitant with decreases in Suc and stachyose, we observed increases in the levels of Glc and Fru from 12 until 72 h. Soybean cotyledons and HRA contained only 1% of dry mass as starch at 12 h. In cotyledons, starch levels increased throughout the experiment and reached 6% by 96 h (Supplemental Fig. S6A), while in the HRA, levels increased to 6% by 48 h before decreasing to 3% at the end of the experiment (Supplemental Fig. S6B).

Gas chromatography-mass spectrometry (GC-MS)-based metabolite profiling was used to detect the activation of processes associated with seed reserve mobilization and changes in abundance of soluble metabolites from 24 h onward. Cotyledons were characterized by increases in the levels of proteinogenic amino acids, likely reflecting the breakdown of protein (Supplemental Fig. S7). Asn showed particularly substantial changes in relative abundance, with levels increasing more than 150 times between 24 and 96 h. Levels of γ-aminobutyric acid (GABA) also increased by around 20-fold by 72 h, and the organic acids fumarate and malate both increased at 96 h, while myo-inositol also showed a gradual increase from 24 to 72 h. In the HRA, we also detected increases in amino acids (Ser, Val, Phe, Gly, Asn, and β-Ala) and organic acids (malate, fumarate, succinate, and malonate; Supplemental Fig. S8). Amino acids and organic acids may constitute a significant proportion of dry mass, and we therefore used NMR spectroscopy to determine the absolute levels of the most abundant of these compounds at 96 h (Supplemental Table S5). Indeed, at 96 h, Asn and citrate represented 1.91% and 1.24% of the dry mass of cotyledons, respectively. The contribution of amino acids and organic acids to the dry mass of the HRA was even greater, with this material containing 5.91%, 1.06%, and 1.82% of dry mass as Asn, GABA, and malate, respectively. To incorporate metabolite data into the metabolic model, the relative changes in metabolite abundance determined using GC-MS were used to back calculate the abundances of the amino acids and organic acids listed in Supplemental Table S5 at 24, 48, and 72 h from the NMR data obtained at 96 h. Other metabolites detected using GC-MS were assumed to make a negligible contribution to total seedling biomass.

FBA and Flux Variability Analysis of Soybean Seedling Metabolism

The experimental mass and composition data were used to calculate constraints for FBA by comparing the total amount of each biomass component at each time

point, leading to three sets of input constraint data expressed on a millimole seedling^{-1} d^{-1} basis (24–48 h, 48–72 h, and 72–96 h). After incorporating the experimental constraints into the multiorgan soybean genome-scale model, flux solutions were obtained using a two-stage optimization procedure. The production of ATP and NADPH for cellular maintenance processes was first maximized with the ratio of ATP to NADPH maintenance costs in both the cotyledon and HRA constrained to a ratio of 3:1 based on the value obtained for Arabidopsis (*Arabidopsis thaliana*) heterotrophic cell cultures under control conditions (Cheung et al., 2013). The ratio of water content in the cotyledon and in the HRA during the 24- to 48-h, 48- to 72-h, and 72- to 96-h periods (12.65:1, 3.24:1, and 1.08:1, respectively) was used as a measure of the relative demands of these organs for ATP and NADPH for cellular maintenance and were used to constrain the ratio of cellular maintenance costs in the cotyledon and the HRA. A second round of optimization was then performed where the sum of absolute flux values was minimized. This second step of flux minimization was based on the assumption of metabolic efficiency (Holzhütter, 2004) and has the advantage of eliminating infinite substrate cycles and resolving parallel pathways in different subcellular compartments (Cheung et al., 2013). The selection of this two-step optimization process was based on several lines of reasoning. First, given that our simulations were constrained using measurements of both input and output fluxes, we assumed that the difference between input and output was used for ATP- and NADPH-consuming maintenance processes. Indeed, in an Arabidopsis model, it was previously shown that when given input and output constraints, maximization of ATP maintenance cost gave predictions close to the measured fluxes (Cheung et al., 2013), and when using the two-step optimization method, predictions of CO_2 from FBA agreed well with those estimated from biomass carbon content and growth analysis (Supplemental Fig. S9). Moreover, when only minimization of total flux was used, without maximization of ATP maintenance cost, FBA predicted the accumulation of metabolites that we did not detect in our metabolite profiling analyses, that ATP maintenance costs were zero and rates of CO_2 release that were below those estimated from biomass carbon content. Feasible solutions were obtained directly using the two-step procedure for the 48- to 72-h and 72- to 96-h simulations. Initially, it was not possible to obtain a solution for the 24- to 48-h period. Analysis of nitrogen balance indicated a deficit of nitrogen in the model during this period. For this reason, we allowed the model to import ammonium (NH4_tx_COT) to complete the balance. It is worth noting that the initial imbalance in nitrogen was minor; the additional nitrogen taken up by the model in the form of NH_4^+ represents only 2% of the total nitrogen demand of the HRA from 24 to 48 h. Initial tests of the results for the 24- to 48-h period also revealed fluxes toward the synthesis of fatty acids in the cotyledons, arising due to the slight increase in levels of this biomass component over this period (Supplemental Fig. S4A). Given that the difference in biomass composition was not statistically significant and the fact that we found no support for such biosynthesis in the literature, we opted to set fluxes toward the production of fatty acids to zero. Flux variability analysis (FVA) was performed following the two-step optimization procedure in order to identify alternative optimal solutions.

The multiorgan model contains a total of 6,051 reactions. Of these, a total of 5,311 were not active during any of the periods tested. Of the remaining reactions, a core set of 409 reactions were active during all periods tested (Supplemental File S3). These reactions include cell wall biosynthesis, amino acid and protein biosynthesis, degradation of certain amino acids, glycolysis, the tricarboxylic acid cycle, and oxidative phosphorylation. Despite the overall greater flux through the metabolic network during the 72- to 96-h period compared with 24 to 48 h, the number of active reactions changed little, with 577 reactions active from 24 to 48 h and 578 from 72 to 96 h. Considering the set of experimental constraints and the use of minimization of total flux as an objective function, the activation of a relatively small proportion of the total number of reactions and the fact that different periods all share a large proportion of their active reactions (>70%) is perhaps unsurprising. A comparison of active reactions suggests that the 48- to 72-h and 72- to 96-h periods are more similar to each other than they are to the earlier 24- to 48-h period (Supplemental Fig. S10). Indeed, the 24- to 48-h period contained the greatest number of unique active reactions (134). Among the unique reactions and processes activated for each period, we identified a mitochondrial pyruvate dehydrogenase and citrate synthase (cotyledons) during the 24- to 48-h period, a series of organic acid transporter reactions, cytosolic 6-phosphogluconate dehydrogenase (cotyledons), and Asn metabolism during the 48- to 72-h period, and part of the cytosolic oxidative pentose phosphate pathway (OxPPP; HRA) during the 72- to 96-h period.

FBA predicted major changes in the metabolic flux distribution between the different growth periods (Fig. 4). In the cotyledons during the 24- to 48-h period (Fig. 4A), sugars released from cell wall and RFO breakdown were mainly used in the synthesis of starch (0.011 mmol seedling^{-1} d^{-1}) and Suc transport to the HRA (0.008 mmol seedling^{-1} d^{-1}), with a small amount fed into the plastidic OxPPP (0.002 mmol seedling^{-1} d^{-1}). The tricarboxylic acid cycle was predicted to operate with stored citrate as a substrate (0.014 mmol seedling^{-1} d^{-1}) as well as acetyl-CoA from pyruvate (0.013 mmol seedling^{-1} d^{-1}). This pyruvate in turn originates almost exclusively from a plastidic and cytosolic NADP-dependent malic enzyme. The main prediction of FVA was the presence of parallel and equivalent routes of citrate conversion to isocitrate in the mitochondria and cytoplasm.

In the HRA (Fig. 4D), sugars arriving in the phloem and from previously accumulated reserves are broken down with part of the carbon used in the synthesis of starch and cell walls. The tricarboxylic acid cycle

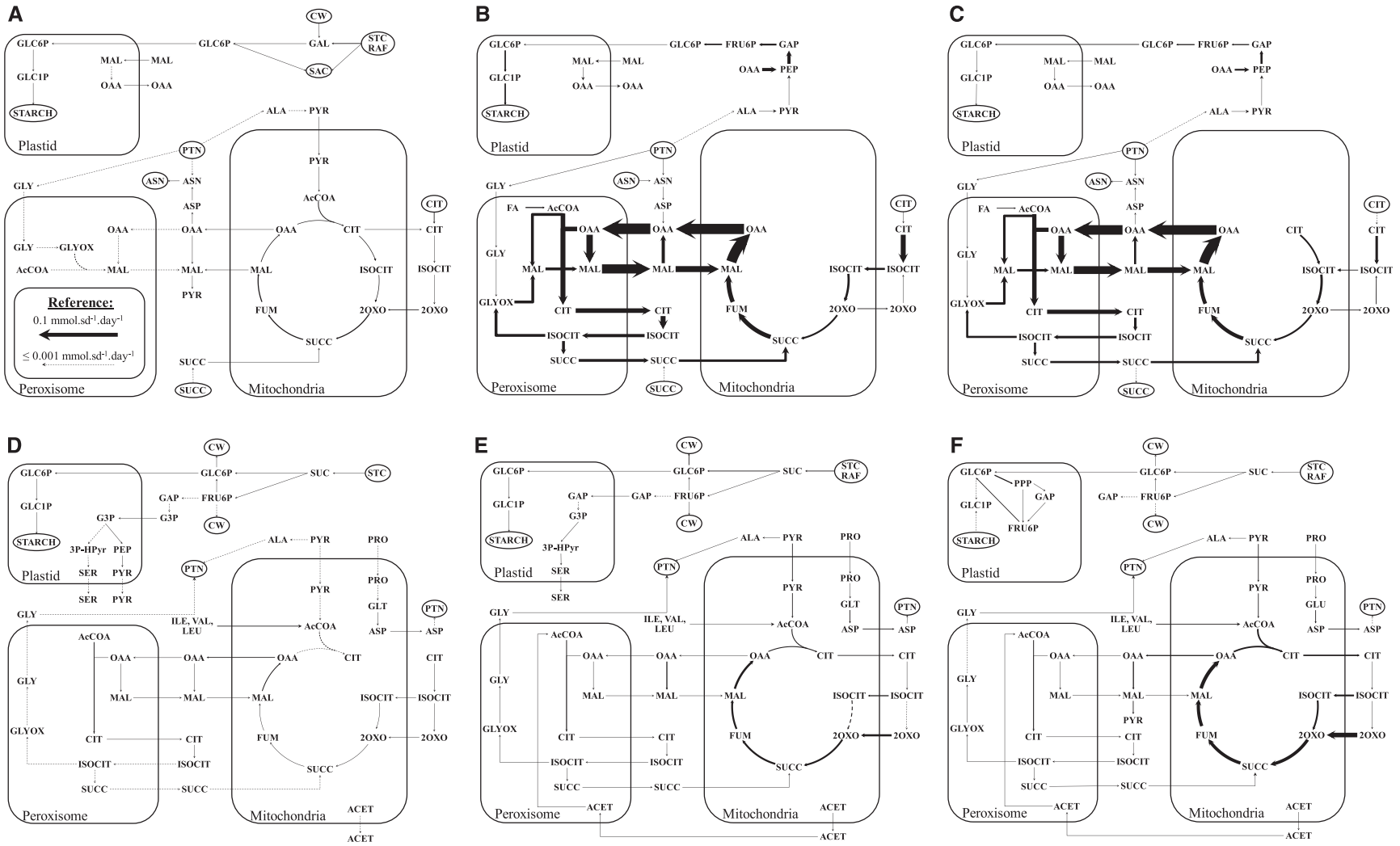

Figure 4. Metabolic fluxes in heterotrophic soybean seedlings predicted using FBA. A and D, Fluxes between 24 and 48 h in cotyledons and HRA, respectively. B and E, Fluxes between 48 and 72 h in cotyledons and HRA, respectively. C and F, Fluxes between 72 and 96 h in cotyledons and HRA, respectively. AcCOA, Acetyl-CoA; ACET, acetate; CIT, citrate; CW, cell wall; FA, fatty acids; FRU6P, Fru-6-P; FUM, fumarate; GAL, Gal; GAP, glyceraldehyde 3-phosphate; GLC1P, Glc-1-P; GLC6P, Glc-6-P; GLYOX, glyoxylate; G3P, 3-phosphoglycerate; H-SER, hydroxy-Ser; ISOCIT, isocitrate; MAL, malate; OAA, oxaloacetate; 2OXO, 2-oxoglutarate; PEP, phospho*enol*pyruvate; 3P-HPyr, 3-phosphohydroxypyruvate; PTN, protein; PYR, pyruvate; RAF, raffinose; STC, stachyose; SUC, Suc; SUCC, succinate. Standard three-letter amino acid abbreviations are used. Biomass components are indicated in ovals. Not all metabolites and fluxes are shown.

operates principally using carbon derived from carbohydrates via glycolysis but also from catabolism of Pro, which also serves to transfer electrons directly to the mitochondrial electron transport chain (mETC).

FBA predictions of metabolism in cotyledons during the 48- to 72-h period (Fig. 4B) were characterized by substantial fatty acid degradation via β-oxidation and operation of the glyoxylate cycle. Part of the peroxisomal acetyl-CoA produced through β-oxidation was used by malate synthase, but the majority (61%) was used in the peroxisomal citrate synthase reaction. Peroxisomal isocitrate was primarily used by isocitrate lyase to produce succinate and glyoxylate, although a proportion (14%) was also degraded by isocitrate dehydrogenase in order to produce the NADPH necessary for the removal of fatty acid double bonds during β-oxidation. Glyoxylate (7% of the total) for the malate synthase reaction was also produced via the transamination of Gly originating from protein hydrolysis. Succinate produced in the peroxisome was ultimately fed, in part, into gluconeogenesis via the conversion of oxaloacetate to PEP via PEP carboxykinase (PEPCK). A small proportion (5%) of PEP was also predicted to be produced from Ala released from protein hydrolysis by the sequential action of Ala aminotransferase and pyruvate orthophosphate dikinase (PPDK). Gluconeogenesis itself was used mainly to provide precursors for starch synthesis, the cytosolic and plastidic OxPPP, and the synthesis of Suc for transport to the HRA. In addition to the parallel routes of citrate-to-isocitrate conversion described above for the 24- to 48-h period, FVA also indicated variability in the proportions of gluconeogenic flux in parallel pathways in the cytoplasm and plastid.

Intermediates of the tricarboxylic acid and glyoxylate cycles were also predicted to be used directly in biosynthetic processes; Glu in particular was formed from cytosolic and peroxisomal 2-oxoglutarate and transported to the HRA, the nitrogen atom being introduced by transamination with Ala, Asp, Gly, or Trp. Peroxisomal citrate was also fed into the mitochondrial tricarboxylic acid cycle, which operated without action of a mitochondrial citrate synthase or pyruvate dehydrogenase. Two oxaloacetate/malate shuttles also acted to transfer NADH from the peroxisomes to the mitochondria for use by the mETC. Since protein synthesis is occurring in the HRA at this point, much of the metabolism observed in this organ was directed toward the production of amino acids and their incorporation into protein (Fig. 4E). Cell walls and starch were also produced using carbon derived from Suc transported from the cotyledons.

ATP demands in the HRA were again met by oxidative phosphorylation. The majority of reductant for mitochondrial electron transport was again produced by the tricarboxylic acid cycle, but, as during the 24- to 48-h period, amino acid catabolism, in this case of Pro, Leu, Ile, and Val, also fed small quantities of electrons into the mETC. FVA suggests that Val degradation could pass electrons to the mETC via either FAD or electron transport flavoprotein (ETF). The main substrate for the tricarboxylic acid cycle was 2-oxoglutarate produced by NADP-dependent Glu dehydrogenase from Glu transported from the cotyledons, while degradation of Pro, Leu, Ile, and Lys also fed carbon into the tricarboxylic acid cycle. Pyruvate dehydrogenase was also operational and used pyruvate produced by plastidic NADP-dependent malic enzyme; no glycolytic flux was predicted.

During the 72- to 96-h period, FBA again predicted that fatty acid breakdown was responsible for the production of acetyl-CoA in the peroxisomes of the cotyledons (Fig. 4C). This acetyl-CoA was again used partly by the glyoxylate cycle (36% directed to malate synthase) and carbon directed to gluconeogenesis via PEPCK (0.049 mmol seedling^{-1} d^{-1}) and to a lesser extent PPDK (0.002 mmol seedling^{-1} d^{-1}), although the rate of PEP production was predicted to be only 63% of that from 48 to 72 h. Instead, a greater proportion of citrate produced in the peroxisomes was used directly in the mitochondrial tricarboxylic acid cycle instead of being used in the glyoxylate cycle, as reflected by a decrease in the ratio of PEPCK to citrate synthase flux from 0.67 to 0.47; again, no citrate was produced directly in the mitochondrion. The tricarboxylic acid cycle was also operational in the HRA, with acetyl-CoA being derived mainly from pyruvate produced by plastidic malic enzyme activity. As in the 48- to 72-h period, the majority of carbon entering the tricarboxylic acid cycle was derived from Glu transported from the cotyledons, while other amino acids, including Pro, Lys, and branched chain amino acids, made smaller contributions. Again, plastidic malic enzyme was the main source of pyruvate, and carbon from Suc breakdown was used in HRA cell wall and starch synthesis (Fig. 4F).

The Impact of Maintenance Energy Assumptions on Flux Predictions

Previous studies have shown that demand for ATP and NADPH for maintenance processes exerts a strong influence on the flux distributions predicted by FBA (Cheung et al., 2013). We therefore carried out a series of simulations where we varied the ATP:NADPH maintenance ratio (from 1:1 to infinity:1; Supplemental Figs. S11–S13) or the relative maintenance demands of the cotyledons and HRA (from 0.5 to 100; Supplemental Figs. S14–S16) before the two-step optimization procedure. Below, we describe how predictions of representative fluxes from key processes identified in the baseline simulations described above (ATP:NADPH 3:1, relative maintenance demands based on water content) were affected by changes in these ratios. In general, alterations in the ATP:NADPH ratio produced few qualitative differences, with the same reactions active over the whole range or only being severely perturbed at extreme values (1:1 or infinity:1). Several effects were observed. During the 24- to 48-h period, flux through the plastidic OxPPP decreased and ceased above a ratio of 3:1 (Supplemental Fig. S11A). Moreover, while total NADP-dependent malic enzyme activity remained

relatively constant, the predominant isoform varied with the ATP:NADPH ratio; at the extremes (1:1, 2:1, and infinity:1), the cytosolic form was most important, while at intermediate values (3:1, 4:1, and 5:1), the cytosolic isoform carried greater flux (Supplemental Fig. S11C). As would be anticipated, an increased ATP:NADPH ratio led to increased tricarboxylic acid cycle flux. HRA metabolism was little affected, likely due to the proportionally lower overall maintenance costs in this organ during this period. Effects of the ATP:NADPH ratio on the 48- to 72-h and 72- to 96-h period were even less pronounced (Supplemental Figs. S12 and S13). In the cotyledons, there was a trend toward increased tricarboxylic acid cycle flux and decreased flux through the glyoxylate cycle, gluconeogenesis, and OxPPP with an increasing ratio. In the HRA, increases in the ratio also led to increased tricarboxylic acid cycle flux and deactivation of the OxPPP. As in the cotyledons during the 24- to 48-h period, FBA predicted alterations in the cytosolic and plastidic NADP-dependent malic enzyme isoforms in the HRA at 48 to 72 h and 72 to 96 h; in the 72- to 96-h period in particular, the plastidic form predominated at higher ratios (4:1, 5:1, and 10:1) and the cytosolic form predominated at lower ratios (2:1 and 3:1). Finally, while PEPCK was active in the cotyledons at all ratios, the PPDK route of PEP production for gluconeogenesis was deactivated at ratios of 10:1 and above.

Similarly, increasing the cotyledon:HRA maintenance ratio from 0.5 to 100, values that bracket those used in the baseline simulation, generally led to gradual changes in fluxes (Supplemental Figs. S14–S16). For each of the periods, an increased ratio led, as would be expected, to decreased HRA tricarboxylic acid cycle flux and increased cotyledon tricarboxylic acid cycle flux. For both the 48- to 72-h and 72- to 96-h periods, an increased ratio led to decreased glyoxylate cycle flux in the cotyledons and decreased NADP-dependent malic enzyme activity in HRA. Interestingly, in HRA during the 72- to 96-h period, high (10:1 and 100:1) ratios led to activation of malate synthase and isocitrate lyase. GAPDH was one of the most clearly affected reactions of those selected. For the 24- to 48-h period, increasing the ratio from 2:1 to 10:1 led to deactivation of the cytosolic isoform and activation of the plastidic isoform in the HRA, while during the 48- to 72-h period, the opposite trend was observed together with increased flux through F16-BP aldolase. The effects of the alterations of both ratios on predictions of phloem transport and NADPH and ATP production and consumption are described in the sections below.

Transport from Cotyledons to the HRA

Growth of the HRA requires the transport of material from the cotyledons via the phloem, and a number of transport reactions in the model were active during the different periods. Overall, transport of carbon increased greatly from the 24- to 48-h period to the 48- to 72-h period, reflecting the increased rate of growth of the seedling at this later point (Supplemental Fig. S17). Similarly, transport of nitrogen increased dramatically after 24 to 48 h as demand for nitrogen for amino acid and protein synthesis in the HRA increased.

The compounds transported varied between the different periods (Supplemental Fig. S18). Suc made the greatest contribution to carbon transport in all three periods, although the percentage contribution decreased from 69% at 24 to 48 h to 30% at 72 to 96 h. Amino acids also made important contributions to carbon transport, with 22% and 25% of carbon being transported in the form of Glu alone during the 48- to 72-h and 72- to 96-h periods, respectively. The greatest contributions to nitrogen transport were made by Arg, Lys, Pro, and Glu (totaling 61%) during the 24- to 48-h period, Asn and Glu (totaling 50%) during the 48- to 72-h period, and Arg, Glu, Lys, and Pro (totaling 71%) during the 72- to 96-h period.

FVA uncovered almost no variation in phloem transport, with only a small degree of flexibility in Glu transport, as a small proportion of Glu could be substituted by GABA (Supplemental Fig. S18). Varying the ATP:NADPH maintenance ratio had a greater quantitative effect for the 48- to 72-h and 72- to 96-h periods. In both cases, a parabolic response of Glu transport accompanied by a proportional hyperbolic response of Suc transport was observed as the ATP:NADPH ratio was increased from 1:1 to exclusively ATP-based maintenance. Unsurprisingly, increases in the cotyledon:HRA maintenance ratio from 0.1 to 10 led to an overall decrease in cotyledon-to-HRA transport, with Suc and Glu transport principally affected.

Consumption and Production of ATP and NADPH

The use of genome-scale modeling permits the analysis of overall cofactor balances and the prediction of the reactions that have an important influence on these balances. In all solutions, FBA predicted that a small set of reactions were responsible for NADPH production in both the cotyledons and HRA (Supplemental Fig. S19). In the cotyledons from 24 to 48 h, 55% of NADPH was produced by cytosolic and mitochondrial isocitrate dehydrogenase (NADP-ICDH), with an additional 26% from cytosolic and plastidic malic enzyme and 10% from the plastidic OxPPP. This pattern shifted over time; during the 48- to 72-h and 72- to 96-h periods, 28% to 29% of NADPH was produced by mitochondrial NADP-ICDH and 57% to 59% by the OxPPP (cytosolic and plastidic).

In the HRA from 24 to 48 h, 57% of NADPH was produced by cytosolic and mitochondrial NADP-ICDH and an additional 31% from the plastidic OxPPP. During the 48- to 72-h period, 35% of NADPH derived from Glu dehydrogenase (GDH) activity, 32% from plastidic malic enzyme, and 27% from mitochondrial NADP-ICDH, while from 72 to 96 h, NADP-ICDH (27%), GDH (22%), and the plastidic OxPPP (30%) were the major

contributors. Consumption of NADPH was dominated (85% to 88%) by maintenance costs in the cotyledons (NADPH oxidase), with a small contribution from the peroxisomal enzymes involved in the removal of fatty acid double bonds and cytosolic NADP-ICDH during the 48- to 72-h and 72- to 96-h periods. In the HRA, the cytosolic NADPH oxidase also consumed the greater part of NADPH (>94%) in the latter two periods. From 24 to 48 h, however, a number of other reactions were also important, including reactions involved in Rha and Fuc synthesis, fatty acid metabolism, and acetolactate reductoisomerase, an enzyme involved in Leu and Val synthesis. FVA indicated almost no variability in NADPH-associated fluxes, with the exception that NADPH production by mitochondrial NADP-ICDH in the HRA could be substituted entirely (24–48 h) or partially (48–72 h) by 1-pyrroline-5-carboxylate dehydrogenase, an enzyme involved in Pro degradation.

As would be expected, alterations in the ATP:NADPH maintenance ratio had significant effects on predictions of the metabolism of NADPH in both the cotyledons and HRA. In the cotyledons and HRA during both the 48- to 72-h and 72- to 96-h periods, the effects of increasing the ATP:NADPH maintenance ratio were mainly quantitative, with a gradual decrease in most NADPH-producing reactions. The main qualitative alterations in the cotyledons were the lack of cytosolic OxPPP flux from a ratio of 5:1 and above and flux through cytosolic NADP-ICDH, which was negative at low ratios and positive at 4:1 and above. In HRA, the pattern of alteration was similar, although here no OxPPP activity, plastidic or cytosolic, was predicted above 2:1 and cytosolic NADP-ICDH was negative at both extremes of the ATP:NADPH ratio. The 24- to 48-h period presented greater qualitative alterations in NADPH metabolism in the cotyledons as the ATP:NADPH ratio increased; however, these were mainly in the form of altered participation of different isoforms of the same enzyme. For example, flux through cytosolic NADP-ICDH increased as that through the mitochondrial isoform decreased. A similar pattern was observed for NADP-malic enzyme, with the cytosolic enzyme more active at extreme ratios and the plastidic isoform active at intermediate ratios. In HRA, the main qualitative variation was that activation of 1-pyrroline-5-carboxylate dehydrogenase was restricted to the 1:1 and 3:1 ratio simulations. Varying the ATP:NADPH ratio had no effect on the prediction that maintenance processes represent the largest sink for NADPH in both the cotyledons and HRA during all periods. Varying the ratio of cotyledon to HRA maintenance processes around the baseline values led to no qualitative changes in the NADPH-producing reactions; the same NADPH-producing processes were activated and deactivated in the cotyledon and HRA, respectively, as the ratio increased. Indeed, when fluxes through identical reactions were summed over the cotyledons and HRA, alterations in the maintenance ratio produced almost no effects on reactions producing NADPH.

As for NADPH, a small number of reactions were also responsible for ATP synthesis. In both the cotyledons and HRA, the majority of ATP (from 86% to 95%) was produced by the mitochondrial ATP synthase. Other significant contributions were made by mitochondrial succinyl-CoA ligase and, in the HRA during the 24- to 48-h period, the glycolytic reactions pyruvate kinase and phosphoglycerate kinase. These last two reactions made no contribution to ATP synthesis in the cotyledons due to the operation of gluconeogenesis. In the cotyledons, the generic ATPase reaction was responsible for the majority of ATP consumption, with values varying between 59% and 70% of the ATP produced in these organs. Other reactions consuming substantial proportions of ATP (>5%) included galactokinase and the production of ADP-Glc during the 24- to 48-h period, while the gluconeogenic PEPCK and phosphoglycerate kinase reactions were important during the latter two periods. The plasma membrane H^+-ATPase consumed between 7% and 9% of ATP during all periods. The generic ATPase generally consumed a smaller proportion of ATP in the HRA than in the cotyledons, ranging between 11% (24–48 h) and 69% (72–96 h). Here, GTP, UTP, and AMP metabolism made an important contribution to ATP usage, together with the plasma membrane H^+-ATPase and protein translocation costs. FVA indicated no variation in fluxes responsible for ATP production, with the exception of partitioning between cytosolic and plastidic phosphoglycerate kinase in the HRA during the 24- to 48-h period.

Increasing the ATP:NADPH maintenance ratio naturally led to predictions of increased ATP synthesis, although the relative importance of the reactions contributing to total synthesis was little affected, the only important qualitative alteration in flux being the increased importance of phosphoglycerate kinase in the HRA at high ratios. As for NADPH synthesis, increasing the cotyledon:HRA maintenance ratio did not alter the identity of the reactions responsible for the production of ATP, with the only exception being the induction of phosphoglycerate kinase activity at low ratios in HRA during the 48- to 72-h and 72- to 96-h periods.

^{13}C Labeling of Soybean Seedlings

To validate the results obtained using FBA, we carried out a stable isotope-labeling experiment where seeds were germinated in liquid medium containing [U-^{13}C]Glc. Incorporation of the ^{13}C label was detected in a number of intermediates of primary metabolism over 4 d of growth (Supplemental Fig. S20). Operation of glycolysis or the pentose phosphate pathway together with operation of the tricarboxylic acid cycle in the HRA was indicated by accumulation of the citrate M+2 isotopomer, likely produced by the entry of carbon into the tricarboxylic acid cycle via acetyl-CoA. Operation of the tricarboxylic acid cycle was also indicated by labeling of fumarate and malate. In comparison, little label was incorporated into citrate in the cotyledons. Given that Glu and malate were labeled in these organs, this implies the existence of a citrate pool that cannot be labeled directly from

[U-^{13}C]Glc, most likely deriving from citrate accumulated in the seed prior to germination and that formed by β-oxidation of fatty acids and the peroxisomal citrate synthase reaction.

DISCUSSION

FBA of Reserve Mobilization in Heterotrophic Soybean Seedlings

FBA using genome-scale stoichiometric models has been demonstrated to be a valuable tool for the study of plant metabolism and is able to generate predictions that closely reflect in vivo flux distributions (Williams et al., 2010; Cheung et al., 2013). Since the creation of the first genome-scale stoichiometric models for Arabidopsis (Poolman et al., 2009), models with similar scope have been produced for a number of commercially important plants, including rice (*Oryza sativa*; Mohanty et al., 2016), tomato (Yuan et al., 2016b), and maize (*Zea mays*; Saha et al., 2011). Here, we report the construction, curation, and testing of a genome-scale model of soybean, a highly important legume crop. The creation of this model should facilitate studies of the metabolism of this species and, due to the associations between genes, reactions and metabolites contained within the model could aid in the interpretation of results obtained using postgenomic techniques. In addition to the investigation of single-cell metabolic phenotypes, FBA has great potential for the study of interactions between different cell types (Dal'Molin et al., 2010), tissues, and organs (Borisjuk et al., 2013; Dal'Molin et al., 2015; Rolletschek et al., 2015; Moreira et al., 2019). By using a multiorgan model together with experimental constraints, we were able to simultaneously model metabolism in both sink and source organs within growing soybean seedlings. The method we employed here using a genome-scale model has the advantage of increasing the power of the FBA analysis to generate new hypotheses regarding metabolic flux distributions. Future extensions of this approach may focus on the creation of submodels for different tissues within each organ, as the different tissues that constitute both sink and source organs are expected to exhibit different metabolic flux phenotypes. This will ultimately require the implementation of technically demanding cell separation, cryosectioning, matrix-assisted laser-desorption ionization-MS imaging (Feenstra et al., 2017), in vivo magnetic resonance imaging techniques (Munz et al., 2017), or cell-specific metabolic flux analysis (Rossi et al., 2017).

FBA predicted major differences in metabolism between the cotyledons and HRA, with alterations occurring throughout the duration of the experiment. Metabolism from 24 to 48 h was characterized by the consumption of previously accumulated reserves of sugars and organic acids. From 48 h onward, fatty acid oxidation in the cotyledons supplied carbon for transport to the HRA in the form of Suc and Glu and for the tricarboxylic acid cycle. During the whole period, amino acids released from protein hydrolysis in the cotyledons were transported to the HRA for both protein synthesis and catabolism. These predictions were supported by ^{13}C-labeling experiments that highlight the presence of a nonlabeled citrate pool in the cotyledons and operation of the tricarboxylic acid cycle. Labeling data also indicated operation of glycolysis and/or the pentose phosphate pathway together with a mitochondrial citrate synthase, and FBA predicted the operation of these processes for all periods in the HRA and in the cotyledons for the 24- to 48-h period. The absence of pyruvate dehydrogenase and mitochondrial citrate synthase activity in the FBA solutions for cotyledons for the 48- to 72-h and 72- to 96-h periods likely reflects the prediction that there is an ample supply of acetyl-CoA in the peroxisome, resulting from β-oxidation, that can be directed to the tricarboxylic acid cycle via peroxisomal citrate synthase activity. FVA indicated very little potential variability in the flux solutions and no alternative optima that would affect our interpretation of the results. Similarly, while alterations in the ATP:NADPH and cotyledon:HRA maintenance ratios produced alterations in the predicted flux distributions, such alterations were mainly quantitative in nature and did not affect our overall interpretation of metabolism in developing soybean seedlings. Individual elements of soybean seedling metabolism are discussed in more detail below.

Carbohydrate Biosynthesis and Catabolism in Soybean Seedlings

While soybeans contained very little starch before germination (Yazdi-Samadi et al., 1977; Supplemental Fig. S6), both the cotyledons and HRA contain significant quantities of soluble sugars (Fig. 3; Supplemental Fig. S5). Soluble sugars, including the RFOs, may be involved in protection of the seeds during desiccation (Black et al., 1996; Bailly et al., 2001; Obendorf et al., 2008) through stabilization of membranes (Crowe et al., 1987) and contribute to seed longevity (Koster, 1991; Buitink et al., 2000). Breakdown of Suc and RFOs is also thought to provide energy during the process of germination (Peterbauer and Richter, 2001). However, many of the functions ascribed to RFOs have not yet been confirmed experimentally (Bentsink et al., 2000; Gurusinghe and Bradford, 2001). Here, soluble sugars appear to be the first of the seed reserves to be used, with decreases in total levels in cotyledons as well as alterations in composition in the HRA over the course of the experiment. In this context, it is interesting that negligible decreases in cotyledon sugars were observed between 12 and 24 h, when the process of germination was completed. Indeed, levels of Suc increased over this period, suggesting that cotyledon sugars do not contribute to energy generation during germination. Changes in the HRA during the same period involved a major decrease in stachyose and increases in Suc, Glc, and Fru, but again, total soluble sugar levels remained constant. It therefore seems likely that other reserves are meeting

energetic demands at this stage, consistent with results obtained using reduced-stachyose soybeans and an RFO degradation inhibitor, where mobilization of RFOs was considered inconsequential for germination (Dierking and Bilyeu, 2009).

Similar patterns of changes in sugar levels have previously been reported for soybean (East et al., 1972; Hsu et al., 1973) and other legumes (McCleary and Matheson, 1974; Buckeridge et al., 1995; Buckeridge and Dietrich, 1996), with decreases in RFOs that were followed by increases in Suc and/or Glc and Fru, although in those studies the decreases in RFOs occurred during germination itself. The breakdown of RFOs in soybean may certainly continue postgermination, as shown by our results and a previous study that revealed the disappearance of raffinose and stachyose after 96 and 144 h, respectively (East et al., 1972). FBA predicts that these sugars contribute to energy generation, starch synthesis, and Suc production for phloem transport postgermination.

Levels of starch in cotyledons and the HRA increased during germination and initial growth (Webster and Leopold, 1977; Adams et al., 1980, 1981; Brown and Huber, 1987; Gronwald et al., 2009). This transitory starch has been suggested to arise from lipid mobilization (Adams et al., 1981), although other research has suggested a connection between decreases in soluble sugar levels, principally raffinose and Suc, and synthesis of starch (Brown and Huber, 1987). Similar relationships between soluble sugars and starch during germination and initial growth have also been reported for mung bean (*Vigna radiata*) and indeed soybean (Kuo et al., 1988). The formation of starch during seedling growth appears to be positively related to growth of the HRA and may act as an internal drain for soluble sugars (Brown and Huber, 1988) as well as a temporary carbon store to be used during a later developmental stage (Colombié et al., 2015).

FBA predicts that carbon for starch synthesis in the cotyledons has different sources at different times following germination. From 24 to 48 h, starch is formed principally from sugars released by cell wall degradation. Cell wall hydrolytic enzymes are known to be produced following germination (Buckeridge et al., 2001), and cell wall breakdown may then release soluble sugars that may be directed toward the formation of transitory starch as well as glycolysis and catabolic processes. Indeed, degradation of cell wall polysaccharides with release of Gal and Ara is known to occur in growing soybean seedlings (Gronwald et al., 2009). The carbon source for cotyledon starch synthesis is altered at 48 to 72 h, with the β-oxidation of fatty acids, the glyoxylate cycle, and gluconeogenesis responsible over this period.

Fatty Acid Degradation and the Metabolic Fates of Peroxisomal Acetyl-CoA

Soybean seeds contain high levels of fatty acids, stored principally in the form of triacylglycerol in the cotyledons, and proteomic and transcriptomic analyses of germinating soybeans and seedlings have indicated the expression of genes coding for enzymes involved in lipid mobilization and degradation (Han et al., 2013; Shamimuzzaman and Vodkin, 2014). Our analysis indicated that around 20% of cotyledon dry mass was composed of fatty acids, with the most abundant being palmitic acid, oleic acid, linolenic acid, and linoleic acid, a similar profile to that in developing cotyledons (Fehr et al., 1971; Allen et al., 2009). Levels of total fatty acids in cotyledons decreased from 48 h onward, and this, combined with decreases in cotyledon mass, indicates that mobilization of fatty acids occurred following germination (Joshi et al., 1973). Indeed, lipids are not thought to be used before or during germination itself, at least when they are not localized in seed endosperm, but instead represent an important reserve during seedling growth when products of their breakdown are transported to the growing tissues (Eastmond et al., 2000; Eastmond and Graham, 2001). Significant decreases in HRA fatty acids occurred from 24 h onward, likely due to their effective dilution caused by an increase in HRA biomass with no apparent de novo fatty acid synthesis.

FBA suggests that fatty acid breakdown plays distinct roles at different times following germination. During the 48- to 72-h and 72- to 96-h periods, fatty acids in cotyledons are degraded via β-oxidation to produce acetyl-CoA that is then fed into the glyoxylate cycle, ultimately leading to the production of PEP that can be used for gluconeogenesis (Canvin and Beevers, 1961; Millhouse et al., 1983; Falk et al., 1998; Graham, 2008; Eastmond et al., 2015). FBA predicted that PEP itself was produced mainly by PEPCK with a small contribution made by PPDK using pyruvate derived from Ala. Experiments using Arabidopsis *ppdk* mutants have given support for the importance of this second route during seed reserve mobilization, principally in the carbon-efficient use of pyruvate derived from amino acid catabolism (Eastmond et al., 2015).

The function of the glyoxylate cycle also has implications for ATP production, as mitochondrial oxidation of succinate to malate leads to the production of substantial quantities of ubiquinol that is subsequently oxidized by the mETC. β-Oxidation within the peroxisome also leads to the production of NADH, and FBA predicts that this NADH is exported to the cytosol and then to the mitochondria by a pair of malate/oxaloacetate shuttles, as is believed to occur in vivo (Graham, 2008). Interestingly, although the model contains the necessary enzymes required to operate the Asp shuttle (peroxisomal Asp aminotransferase, transporters for Glu, Asp, and 2-oxoglutarate) that has previously been proposed (Mettler and Beevers, 1980), the malate/oxaloacetate shuttle was used in all flux solutions, most probably because it makes a smaller contribution to the total sum of fluxes. During the 48- to 72-h and 72- to 96-h periods, degradation of fatty acids in the cotyledons also functioned to support respiration, and indeed, modeling suggested no entry of carbon into the tricarboxylic acid cycle via pyruvate dehydrogenase, with reductant for the mETC being produced via catabolism of tricarboxylic

acid cycle intermediates and via β-oxidation itself. This function of fatty acid degradation as a source of acetyl-CoA for respiration during postgerminative growth has been proposed previously for oleaginous species (Salon et al., 1988; Raymond et al., 1992) and associated with reserve tissues and organs such as cotyledons that form part of the growing seedling, where demand for respiratory substrate is likely to be similar to or greater than that for sugars to be transported to other cells (Eastmond and Graham, 2001; Baker et al., 2006). Indeed, seeds of Arabidopsis lacking peroxisomal citrate synthase are unable to germinate in the absence of exogenous sugars (Pracharoenwattana et al., 2005). This situation can be contrasted with endosperm tissue, where rapid conversion of oil to sugar and its transport to the embryonic axis are of crucial importance to the seedling.

Amino Acid Transport, Biosynthesis, and Catabolism

Protein represents the most abundant reserve in soybean seeds, and its mobilization through the activity of proteases and proteasome systems (Han et al., 2013) has important consequences for the carbon, nitrogen, and sulfur balance of developing seedlings. Nitrogen as a percentage of cotyledon dry mass actually increased from 12 to 72 h before decreasing at 96 h. However, the degradation of cotyledon protein and transport of nitrogen to the HRA was revealed by the overall decrease in cotyledon dry mass, as well as the fact that an increasing proportion of organ dry mass was made up of soluble amino acids (Han et al., 2013).

Amino acids released by protein degradation in the cotyledons may be used in the synthesis of new protein, either in the cotyledons or HRA, or may be subject to degradation to provide carbon skeletons, nitrogen, and sulfur for other metabolic processes (Hildebrandt et al., 2015). FBA predicted the transport of a number of different proteinogenic amino acids from cotyledons to the HRA. Glu was predicted to be quantitatively the most important, and this amino acid is routinely found in soybean phloem sap (Housley et al., 1979; Lima and Sodek, 2003; Vitor et al., 2018).

During the 48- to 72-h and 72- to 96-h periods, significant quantities of Ile, Leu, Val, Lys, Pro, Arg (72–96 h only), and Asn (48–72 h) were also predicted to be transported, of which Ile, Leu, Val, and Asn have previously been detected in soybean phloem sap (Muller and Touraine, 1992). Despite Asp and Ser being routinely described in the literature, FBA did not predict the transport of these amino acids under any of the conditions considered. Amino acid degradation in the HRA was also predicted and was most apparent during the 48- to 72-h and 72- to 96-h periods, with the branched chain amino acids (Val, Leu, and Ile), Lys, Pro, Thr, and Glu principally involved. Branched chain amino acid degradation feeds electrons into the mETC via an ETF (Araújo et al., 2010), and degradation of such amino acids also contributes to energy generation by the addition of acetyl-CoA and succinyl-CoA to the tricarboxylic acid cycle (Araújo et al., 2011). The model also predicts degradation of Lys via the α-amino adipate pathway to contribute to the pool of peroxisomal acetyl-CoA (Stepansky and Galili, 2003). Glu catabolism was particularly important, with this amino acid responsible for the transport of large quantities of both carbon and nitrogen to the HRA. Degradation occurred via an NADP-dependent Glu dehydrogenase, producing 2-oxoglutarate and making an important contribution to NADPH production (Supplemental Fig. S19B). Soybean seedlings are known to contain at least three GDH isoforms (Turano et al., 1996), and in other species, this enzyme is thought to be involved principally in the supply of carbon to the tricarboxylic acid cycle (Robinson et al., 1991; Fontaine et al., 2012).

Carbon and Cofactor Balances during Soybean Seedling Growth

FBA predicts substantial shifts in metabolism during postgerminative growth (Fig. 4), with general trends toward increased flux through the metabolic network, although with little change in the total number of active reactions and the maintenance of a core set of reactions during all periods (Supplemental Fig. S10). Modeling predicts that 69%, 63%, and 51% of carbon released from seedling reserves is used for the synthesis of new biomass during the 24- to 48-h, 48- to 72-h, and 72- to 96-h periods, respectively, with the rest being released in the form of CO_2. These values agree well with our estimates of CO_2 release made using dry mass and percentage carbon abundance data (Supplemental Fig. S20) and are similar to values obtained for heterotrophic Arabidopsis cell suspensions (58%; Williams et al., 2010), sunflower (*Helianthus* spp.) embryos, and maize embryos, although, as would be anticipated, lower than those for green Arabidopsis (80%), soybean (83%), and rapeseed (*Brassica napus*) embryos (>86%; Chen and Shachar-Hill, 2012). The gradual decrease in carbon use efficiency we detected probably reflects the increased total fresh mass of the seedlings by the end of the experiment; a greater volume of metabolically active tissue is likely to demand more resources for cellular maintenance, leaving less to be invested in the production of new biomass, as we discuss in more detail below.

During all periods, the majority of ATP was produced via oxidative phosphorylation in the mitochondria. While the tricarboxylic acid cycle was consistently active, FBA highlights the importance of additional sources of reducing power for the mETC. Malate/oxaloacetate shuttles acting to import NADH into the mitochondria were active during all phases but particularly evident from 48 h onward, when β-oxidation in the cotyledons generated large quantities of NADH. For example, the malate/oxaloacetate shuttle operating between peroxisome and mitochondria during the 48- to 72-h and 72- to 96-h periods was responsible for supplying 50% to 51% of the NADH used by complex I. Electrons derived directly from amino acid catabolism also made a small

contribution, with 5% of ubiquinol in the HRA from 72 to 96 h being produced via ETF.

FBA models typically incorporate an ATP/NADPH maintenance cost that is used to reflect processes that are not explicitly modeled but that contribute to ATP and NADPH consumption (Cheung et al., 2013; Nikoloski et al., 2015). Due to the difficulty associated with the measurement of such costs, our baseline FBA incorporated an ATP:NADPH maintenance cost ratio of 3:1 and a relative maintenance cost between the hypocotyl and cotyledon based on water content. Given the potential impact that these ratios could have on our conclusions, we performed two sensitivity analyses, varying both ratios over a wide range and observing the effects on the flux predictions. While alterations in the flux distribution occurred, these were generally quantitative in nature and did not affect our overall interpretation of metabolism during soybean seedling growth. These simulations do, however, reinforce the importance of the correct treatment of maintenance costs for the prediction of metabolic fluxes using FBA, an area that is beginning to receive greater attention in the plant FBA literature. The incorporation of novel experimental data, including measurement of critical fluxes using ^{13}C metabolic flux analysis (Cheung et al., 2013) and gas-exchange and other physiological parameters (Rolletschek et al., 2015), will ultimately facilitate the determination of key maintenance costs.

FBA analysis of soybean seedlings predicted that a significant proportion of ATP was used for maintenance, with overall seedling values ranging from 50% to 67%. These values can be compared with those for Arabidopsis cell suspension cultures (33%, 13%, and 79%, for control, hyperosmotic, and heat treatments, respectively; Cheung et al., 2013), barley (*Hordeum vulgare*) endosperm/embryo (60%; Rolletschek et al., 2015), rapeseed embryos (44%–48%; Hay and Schwender, 2011), tomato fruit (22%–29%; Colombié et al., 2015), and sunflower embryos (89%, of which less than 20% is due to futile cycling; Alonso et al., 2007). Thus, while the values we obtained were relatively high, they are compatible with those previously reported. Importantly, ATP maintenance costs also lump together costs associated with various biochemical processes that are not explicitly modeled. These include the synthesis of nucleic acids, the transport of mineral ions in the phloem, and protein turnover, which can potentially entail a substantial energetic cost (see discussion in Arnold and Nikoloski, 2014) and is likely to be of particular importance in seedlings where gene expression patterns alter during postgerminative growth (Shamimuzzaman and Vodkin, 2014). In addition, activation of alternative mETC components will decrease ATP production and hence the amount of ATP consumption assigned to maintenance. NADH oxidation by non-proton-pumping NADH dehydrogenases was included in models of tomato fruit metabolism (Colombié et al., 2015, 2017), and alternative mETC components are also likely to be relevant in soybean seedlings. Alternative oxidase (AOX) pathway engagement in soybean seedling roots increases from 5% to 35% between 4 and 7 d of growth (Millar et al., 1998). Similarly, total AOX capacity increases following germination in soybean cotyledons, and uncoupling protein has also been detected in this tissue (Daley et al., 2003), and it may be that these proteins facilitate the oxidation of succinate produced via the glyoxylate cycle (Day et al., 1988). The percentage of NADPH consumption for maintenance, including antioxidant metabolism among other processes, varied between 84% and 90% at the whole seedling level. While these values are high compared with the very low value estimated for barley (1%; Rolletschek et al., 2015) and that estimated for Arabidopsis cell cultures under control conditions (50%; Cheung et al., 2013), they are similar to the value predicted for the Arabidopsis cell culture system under heat treatment (90%), meaning that they are physiologically reasonable.

At present, few points of comparison for NADPH costs are available, although this should change in the future as these potential costs are more routinely assessed using FBA. It is also clear that there is extensive variation in the predicted ATP and NADPH maintenance costs that are reported in the literature, and this likely has three different but interrelated causes: model completeness, modeling assumptions, and physiology. Regarding model completeness, studies have indicated that intracellular transport processes represent significant sinks for ATP (Cheung et al., 2013), and models with limited compartmentation, such as those used in metabolic flux analysis studies, will therefore tend to overestimate ATP maintenance costs. A variety of objective functions have also been used in plant FBA studies, including minimizing total flux, minimizing nutrient uptake, maximizing biomass production, and minimizing metabolic adjustment (Yuan et al., 2016a). Furthermore, many studies have included ATP maintenance costs but not NADPH costs (Poolman et al., 2009; Dal'Molin et al., 2010, 2015; Saha et al., 2011). Finally, a large variation in maintenance costs between different species, organs, and conditions is to be expected. Indeed, a large variation (13% to 79%) has previously been identified for Arabidopsis cell cultures grown under different conditions, and we would also expect differences depending on the extent to which growth is occurring. For example, in a nongrowing system, the vast majority of ATP and NADPH consumption will be assigned to maintenance costs. In this regard, seedlings represent an interesting system, as they contain both sink and source tissues, where the dry mass of the source is substantially greater than that of the sink, and the total mass of the system decreases over time (Fig. 2). While ATP and NADPH may be required for growth purposes in the sink, demand will naturally be lower in the source, where no net growth is taking place, and a greater proportion of ATP and NADPH will be used for maintenance than in an isolated embryo or cell culture during exponential growth under nonstressed conditions, where cells are geared toward the accumulation of biomass.

CONCLUSION

Quantitative studies of metabolic flux during seedling growth are rare, partly due to the difficulties associated with isotope labeling of tissues that contain substantial reserves of carbon and nitrogen, and few examples are found in the literature (Salon et al., 1988). Our experimental and FBA data point to a substantial shift in metabolism around 48 h after the beginning of imbibition, with activation of gluconeogenesis in the cotyledons and substantial amino acid catabolism in the developing hypocotyl root axis. Overall, FBA using a new genome-scale stoichiometric model of soybean metabolism appears to be a useful tool for the investigation of metabolic fluxes during mobilization of seedling reserves, with future applications including the rational metabolic engineering of this species and the modeling of interactions between soybean and nitrogen-fixing bacteria.

MATERIALS AND METHODS

Construction and Curation of a Soybean Genome-Scale Metabolic Model

Construction and Curation of a Draft Model

An initial reaction set for soybean (*Glycine max*) metabolism was obtained from SoyCyc version 6.0 (Plant Metabolic Network; http://www.plantcyc.org/databases/soycyc/6.0) and used to build a model in CobraPy format (Ebrahim et al., 2013). A total of 3,536 reactions were extracted from the database along with genes, enzymes, pathways, and empirical formulae of most metabolites as our initial raw data set. In order to obtain accurate predictions of metabolic fluxes, genome-scale metabolic models should be curated to satisfy multiple criteria, including mass, charge and energy conservation, and thermodynamic feasibility (Thiele and Palsson, 2010). These criteria were all addressed during our model construction and curation processes. First, a set of 1,261 reactions were identified as imbalanced (atomic mass and/or charge) in the raw data set, most of them involving the lack of an empirical formula for at least one metabolite; in these cases, generic metabolite names had typically been used. Among these, 1,029 reactions were removed and the remaining were curated using information available in different databases and the literature to yield our first draft mass and charge balanced model. Reaction directionalities were corrected based on an Arabidopsis (*Arabidopsis thaliana*) genome-scale metabolic model (Cheung et al., 2013) and plant databases. Gaps (missing reactions and/or metabolite name ambiguities) were identified for some of the monosaccharide and oligosaccharide synthesis and amino acid/polymer degradation pathways. These gaps were filled based on evidence from the literature, online reaction databases (MetaCyc, KEGG, and PlantCyc), and previously published plant metabolic models. A detailed description of these gap-filling reactions is available in Supplemental File S4.

Subcellular Compartmentalization

Five subcellular compartments, namely cytosol (_c), mitochondria (_m), plastid (_p), peroxisome (_x), and vacuole (_v), are included in the soybean model, where respective suffixes were used at the end of the reaction and metabolite identifiers to distinguish one compartment from another. The cytosol is the default compartment, and any metabolic exchanges between compartments will go through the cytosol using intracellular exchange reactions between the cytosol and other compartments denoted with the subscripts _pc, _mc, _xc, and _vc for plastidial, mitochondrial, peroxisomal, and tonoplast exchanges, respectively. The information on subcellular compartmentation and intracellular transporters and the energetics associated with transport was obtained from an Arabidopsis genome-scale metabolic model that has undergone extensive curation (Cheung et al., 2013). To model the inputs and outputs of the metabolic system, 18 extracellular exchange reactions and 109 biomass drain reactions were defined using _tx and _biomass, respectively, as the subscripts. Extracellular exchange reactions include various forms of energy sources (Glc, Suc, starch, lipid, and photon) and mineral nutrients (NO_3, NH_4, SO_4, Pi, Ca, Fe, Mg, and K) as inputs along with CO_2, oxygen, water, and proton exchanges with the environment.

Model Testing

The soybean genome-scale model was tested for the production of all biomass components under phototrophic and heterotrophic conditions. In phototrophic conditions, a photon influx was allowed from the photon input reaction (Photon_tx) with active photorespiration and with all organic sources of energy set to zero. Mineral nutrients were allowed to exchange with the environment. The heterotrophic condition was modeled by setting photon influx to zero and allowing Glc as the carbon and energy input (GLC_tx), with all other constraints the same as in the phototrophic condition. With CO_2, oxygen, water, and proton exchanges, the model was able to produce all biomass components under both phototrophic and heterotrophic conditions, with nitrate or ammonia as the sole or combined nitrogen sources.

Reactions to Account for Cellular Maintenance Costs

ATP and NADPH are essential to supply energy and reducing power for the production of biomass. However, a sizable proportion of ATP and NADPH produced by plant cells is required for the maintenance of cellular function (Masakapalli et al., 2010; Cheung et al., 2013). To account for these cellular maintenance requirements, generic ATPase and NADPH oxidase reactions were included in the model, as described by Cheung et al. (2013). NADPH oxidase steps were considered in four different compartments, namely the cytosol, plastid, mitochondria, and peroxisome. A nonzero flux from these generic reactions indicates that the model will produce extra ATP and NADPH beyond that required for biomass production and transport that can be used for maintenance processes. The ATPase and NADPH oxidase reactions were used to test for energy conservation and transhydrogenase cycles as described in Supplemental Methods.

Additional Reactions for Mobilization of Seed Reserves

To model the mobilization of seed reserves, several reactions were added. In lipid mobilization, we added ATP-coupled transport of fatty acids into the peroxisome compartment (Graham, 2008), where the fatty acids are then activated to their acyl-CoA derivatives (Linka and Weber, 2010). β-Oxidation of individual saturated (Baker et al., 2006) and unsaturated (Graham, 2008) fatty acids to acetyl-CoA was also added. Analysis of the biomass data indicated the synthesis of fatty acids at certain time points; reactions were therefore added to reflect the synthesis of C20:0 (Fatland et al., 2005) as well as linoleic and linolenic acids (Harwood, 1996).

Preliminary testing indicated that a number of amino acid degradation pathways were incomplete. We therefore added a series of reactions to fill gaps in these pathways and permit transport between organelles as necessary (Supplemental File S4), using online databases and recent literature as principal sources of information (Cheung et al., 2013; Hildebrandt et al., 2015). Little information regarding the degradation of His in plants is available; for this reason, we allowed transport and unbounded efflux of this amino acid. Further alterations included a reaction necessary to permit the degradation of verbascose. Finally, the model was allowed to accumulate several compounds resulting from the incomplete breakdown of biomass components. A complete description of the changes made to the model is given in Supplemental File S4, together with the references therein, and the model itself is also available as Supplemental File S1.

Multiorgan Cotyledon and Hypocotyl Model

The final soybean model was used to construct a multiorgan cotyledon and HRA model by duplicating each of the reactions and metabolites with labels _COT and _HRA after the compartmentation suffix. Reactions reflecting the transport of metabolites from cotyledon to HRA in the phloem were then added (with suffix _PHL). We opted to permit the model to transport all of the proteinogenic amino acids as well as GABA together with Suc (Fig. 1A). The selection of these metabolites was based on literature information regarding phloem transport in soybean (Peterson et al., 1977; Thorne, 1982; Muller and Touraine, 1992; Weise et al., 2000; Lima and Sodek, 2003; Silva et al., 2003; Vitor et al., 2018) and plants in general (Komor et al., 1996; Lalonde et al., 2003, 2004). We assumed that metabolite loading into the phloem involved active transport (Burley, 1961; Servaites et al., 1979; Komor et al., 1996; Lalonde et al., 2003, 2004).

Growth and biomass composition data were incorporated into the model as described below. To facilitate the mobilization and/or (re)storage of carbon and mineral reserves in the seedling tissues, the hydrolysis of cell wall and protein (denoted using _tx) as well as their biosynthesis (denoted using _biomass) were included in both the cotyledon and HRA submodels (Supplemental File S2). FBA simulations were carried out as described in "Results" using CobraPy (Ebrahim et al., 2013), and results were visualized using the FluxMap (Rohn et al., 2012) plugin for VANTED (Junker et al., 2006).

Plant Material and Seedling Growth

Soybean variety BR/MG46 (Conquista) seeds were used for all experiments. Seeds were washed three times in distilled water before transfer to plastic pots (10 seeds per pot) lined with moistened cotton wool and filter paper (LeVan et al., 2008). Seeds were then covered with 200 g of washed humid sand, and pots were transferred to an incubator and maintained in the dark at 25°C until harvest. Five pots of seedlings were harvested at 12, 24, 48, 78, and 96 h (Fig. 1B). At each harvest point, the seedlings from each pot were manually dissected into the cotyledons (without seed coat) and HRA; these organs were then weighed before snap freezing in liquid nitrogen and storage at −80°C. The separate organs were freeze-dried for 48 h and weighed again to determine the dry mass.

Analysis of Seedling Biomass Composition

Soluble sugars were extracted using 80% (v/v) ethanol at 80°C (Praxedes et al., 2006) and quantified using an anion-exchange HPLC device equipped with a pulsed amperometric detector (ICS 3000; Dionex) and Carbopak PA-10 column. Sugars were separated using an isocratic method (74% [v/v] water and 26% [v/v] 200 mM NaOH) over 35 min with a column flow of 0.2 mL min^{-1}. Starch in the insoluble fraction remaining after extraction of soluble sugars was quantified using an enzymatic protocol (Amaral et al., 2007). Total carbon and nitrogen were determined via the combustion of biomass using a carbon/nitrogen/sulfur analyzer (CN-628S; Leco). Samples were dried for more than 12 h at 60°C before being transferred to tin cups and weighed; 100 mg of dry cotyledon and 15 to 20 mg of HRA material were used. Combustion was carried out in an excess of pure oxygen at 950°C, and helium was used as the carrier gas. The equipment was calibrated using certified orchard leaf (Leco 502-055; 44%–52% C and 2%–2.8% N) and Phe standards (Leco 502-642; 65.4% C and 8.5% N). Fatty acids in dry biomass were converted to their methyl esters (FAMES) using a hydrochloric acid/methanol in situ method adapted from Laurens et al. (2012). Samples were analyzed on a GC-MS device (Agilent; 7890-5975) equipped with a 30-m INNOWAX (Agilent Technologies) capillary column. One microliter of sample was injected with an injector temperature of 250°C and a split ratio of 30:1. Separation was achieved using 1 mL mL^{-1} constant helium gas flow and a temperature program starting at 70°C, ramping to 130°C at 20°C min^{-1}, and then to 260°C at 10°C, before maintaining the final temperature for 5 min. Quantification was carried out using the Agilent ChemStation software, and standard curves were constructed using a certified mixture of FAMES (Grain FAME standard; Sigma-Aldrich). Extraction, derivatization, and analysis of samples for metabolite profiling followed a modified method for GC-MS-based metabolite profiling (Lisec et al., 2006). Chromatograms were aligned using the software MetaAlign (Lommen, 2009), and the relative abundance of compounds was determined using ions specific for each compound of interest. Data were visualized using VANTED (Junker et al., 2006). Absolute concentrations of metabolites were determined using NMR spectroscopy. Dried methanolic extracts were dissolved in a buffer containing 1 mM trimethylsilyl-2,2,3,3-tetradeuteropropionic acid sodium salt, 1 mM EDTA, 50 mM KH_2PO_4, and 50 mM K_2HPO_4 in deuterated water. Samples were analyzed on a Bruker Ascend 600-MHz instrument equipped with a double resonance broadband probe. 1D ^1H spectra were acquired using a pulse sequence including a 30°C pulse, 2.73-s acquisition time, and 7-s relaxation delay with 128 scans. Spectra were processed and integrated using the ACD Labs 1D NMR processor, and metabolites were quantified relative to the trimethylsilyl-2,2,3,3-tetradeuteropropionic acid sodium salt signal. Additional details are given in the supporting information (Supplemental Methods).

^{13}C-Labeling Experiments

Soybean seeds were germinated and seedlings were grown in 10 mL of liquid medium containing 20 mM MES (pH 6.5), 10 mM Glc, and 10 mM [U-^{13}C]Glc in 50-mL Erlenmeyer flasks. Seedlings were grown for 1 to 4 d in the dark in a shaking incubator at 25°C before harvest as described above. Incorporation of ^{13}C was assessed using GC-MS analysis of polar metabolites as described in the section "Analysis of Seedling Biomass Composition". Mass isotopomer abundances were corrected for natural abundance isotopes using the tool IsoCor (Millard et al., 2012).

Incorporation of Growth and Biomass Composition Data into the Metabolic Model

Growth and biomass composition data were incorporated into the model in the form of constraints on input and output fluxes (Supplemental Table S6). The relative abundance of each biomass component (g g^{-1} dry weight) at each time point was first multiplied by the mass of the organs collected at that point to determine the total amount of each biomass component on a seedling basis. Flux constraints were then determined by calculating the difference in the quantity of each biomass component between the different time points. While measurements of soluble sugars, amino acids, organic acids, starch, and fatty acids could be incorporated into the model directly, the composition of other biomass components was taken from the literature. The composition of soybean cell walls has previously been measured (Ouhida et al., 2002), and studies have also indicated that Ara and Gal are the principal sugars released during soybean cell wall degradation during germination (Gronwald et al., 2009; Supplemental Table S7). Results obtained through elemental analysis represent the total nitrogen in a sample and thus include nitrogen encountered in protein, free amino acids, and nucleic acids among other compounds. To estimate the amount of protein necessary for metabolic modeling, we first subtracted from total nitrogen the contribution of free amino acids measured using NMR and GC-MS. The contributions of other compounds to total nitrogen were assumed to be negligible. Protein was then estimated using a published nitrogen-to-protein conversion factor for soybean (5.71; Greenfield and Southgate, 2003). The amino acid composition of soybean cotyledon protein was taken from work carried out on a Brazilian variety with a similar 100-grain weight (Vieira et al., 1999; Supplemental Table S8). The amino acid composition of HRA protein was taken from previously published data on soybean hypocotyls grown under similar conditions (Gamborg and Finlayson, 1969; Supplemental Table S8). Finally, we assumed a stoichiometric relationship of 3:1 between fatty acid and glycerol abundance.

Accession Numbers

Accession numbers of the genes and proteins discussed in this article are given in Supplemental File S1.

Supplemental Data

The following supplemental materials are available.

Supplemental Figure S1. Dry mass as a percentage of fresh mass in cotyledons and HRA in soybeans at different times following the beginning of imbibition.

Supplemental Figure S2. Levels of carbon as a percentage of dry mass in cotyledons and HRA in soybeans at different times following the beginning of imbibition.

Supplemental Figure S3. Levels of nitrogen as a percentage of dry mass in cotyledons and HRA in soybeans at different times following the beginning of imbibition.

Supplemental Figure S4. Levels of FAMES as a percentage of dry mass produced from cotyledons and HRA in soybeans by transesterification at different times following the beginning of imbibition.

Supplemental Figure S5. Levels of total soluble sugars as a percentage of dry mass in cotyledons and HRA in soybeans at different times following the beginning of imbibition.

Supplemental Figure S6. Levels of starch as a percentage of dry mass in cotyledons and HRA in soybeans at different times following the beginning of imbibition.

Supplemental Figure S7. Metabolic profiling of cotyledons of soybeans from 24 to 96 h after the beginning of imbibition.

Supplemental Figure S8. Metabolic profiling of HRA of soybeans from 24 to 96 h after the beginning of imbibition.

Supplemental Figure S9. Carbon conversion in soybean seedlings during different growth periods following the beginning of imbibition.

Supplemental Figure S10. Venn diagram indicating the number of activated reactions shared between FBA simulations of different periods following the beginning of imbibition of soybean seeds.

Supplemental Figure S11. Effect of variation of the ATP:NADPH maintenance ratio on selected metabolic fluxes for the 24- to 48-h period.

Supplemental Figure S12. Effect of variation of the ATP:NADPH maintenance ratio on selected metabolic fluxes for the 48- to 72-h period.

Supplemental Figure S13. Effect of variation of the ATP:NADPH maintenance ratio on selected metabolic fluxes for the 72- to 96-h period.

Supplemental Figure S14. Effect of variation of the cotyledon:HRA maintenance ratio on selected metabolic fluxes for the 24- to 48-h period.

Supplemental Figure S15. Effect of variation of the cotyledon:HRA maintenance ratio on selected metabolic fluxes for the 48- to 72-h period.

Supplemental Figure S16. Effect of variation of the cotyledon:HRA maintenance ratio on selected metabolic fluxes for the 72- to 96-h period.

Supplemental Figure S17. Cotyledon-to-HRA transport of carbon and nitrogen predicted by FBA during the different simulation periods.

Supplemental Figure S18. Cotyledon-to-HRA transport of sugars and amino acids during the different simulation periods.

Supplemental Figure S19. Percentage contribution of different reactions to total NADPH production in soybean cotyledon and HRA during different growth periods following the beginning of imbibition.

Supplemental Figure S20. Incorporation of ^{13}C in metabolites extracted from soybean seedlings incubated with U-^{13}C-labeled Glc.

Supplemental Table S1. Levels of fatty acids in soybean cotyledons at different times following the beginning of imbibition.

Supplemental Table S2. Levels of fatty acids in soybean HRA at different times following the beginning of imbibition.

Supplemental Table S3. Levels of sugars in soybean cotyledons at different times following the beginning of imbibition.

Supplemental Table S4. Levels of sugars in soybean HRA at different times following the beginning of imbibition.

Supplemental Table S5. Levels of amino acids and organic acids in soybean cotyledons and HRA at 96 h following the beginning of imbibition determined using NMR analysis of tissue extracts.

Supplemental Table S6. Sources of data for calculation of exchange fluxes.

Supplemental Table S7. Cell wall monomer abundance and stoichiometric coefficients for reactions describing the synthesis and hydrolysis of cell walls in the FBA model.

Supplemental Table S8. Amino acid percentage abundance in protein and stoichiometric coefficients for reactions describing the synthesis and hydrolysis of protein in the FBA model.

Supplemental File S1. Genome-scale metabolic model of soybean.

Supplemental File S2. Multiorgan model of soybean seedling metabolism.

Supplemental File S3. Flux data: parsimonious FBA, FVA, and sensitivity analysis solutions.

Supplemental File S4. Additional and curated reactions.

Supplemental Methods. Additional methods and references.

ACKNOWLEDGMENTS

We thank Francisco Aragão (Embrapa Cenargen) for the generous donation of the seeds, Raquel Azevedo (University of Brasília) for help establishing the analytical protocols, and the University of Brasília NMR facility.

Received January 30, 2019; accepted May 25, 2019; published June 10, 2019.

LITERATURE CITED

Adams C, Rinne R, Fjerstad M (1980) Starch deposition and carbohydrase activities in developing and germinating soya bean seeds. Ann Bot **45:** 577–582

Adams C, Broman T, Rinne R (1981) Starch metabolism in developing and germinating soya bean seeds is independent of β-amylase activity. Ann Bot **48:** 433–440

Allen DK, Ohlrogge JB, Shachar-Hill Y (2009) The role of light in soybean seed filling metabolism. Plant J **58:** 220–234

Alonso AP, Goffman FD, Ohlrogge JB, Shachar-Hill Y (2007) Carbon conversion efficiency and central metabolic fluxes in developing sunflower (*Helianthus annuus* L.) embryos. Plant J **52:** 296–308

Amaral LIV, Gaspar M, Costa PMF, Aidar MPM, Buckeridge MS (2007) Novo método enzimático rápido e sensível de extração e dosagem de amido em materiais vegetais. Hoehnea **34:** 425–431

Araújo WL, Ishizaki K, Nunes-Nesi A, Larson TR, Tohge T, Krahnert I, Witt S, Obata T, Schauer N, Graham IA, et al (2010) Identification of the 2-hydroxyglutarate and isovaleryl-CoA dehydrogenases as alternative electron donors linking lysine catabolism to the electron transport chain of Arabidopsis mitochondria. Plant Cell **22:** 1549–1563

Araújo WL, Tohge T, Ishizaki K, Leaver CJ, Fernie AR (2011) Protein degradation: An alternative respiratory substrate for stressed plants. Trends Plant Sci **16:** 489–498

Arnold A, Nikoloski Z (2014) Bottom-up metabolic reconstruction of Arabidopsis and its application to determining the metabolic costs of enzyme production. Plant Physiol **165:** 1380–1391

Bailly C, Audigier C, Ladonne F, Wagner MH, Coste F, Corbineau F, Côme D (2001) Changes in oligosaccharide content and antioxidant enzyme activities in developing bean seeds as related to acquisition of drying tolerance and seed quality. J Exp Bot **52:** 701–708

Baker A, Graham IA, Holdsworth M, Smith SM, Theodoulou FL (2006) Chewing the fat: β-Oxidation in signalling and development. Trends Plant Sci **11:** 124–132

Bentsink L, Alonso-Blanco C, Vreugdenhil D, Tesnier K, Groot SPC, Koornneef M (2000) Genetic analysis of seed-soluble oligosaccharides in relation to seed storability of Arabidopsis. Plant Physiol **124:** 1595–1604

Bewley JD (1997) Seed germination and dormancy. Plant Cell **9:** 1055–1066

Black M, Corbineau F, Grzesikit M, Guyi P, Côme D (1996) Carbohydrate metabolism in the developing and maturing wheat embryo in relation to its desiccation tolerance. J Exp Bot **47:** 161–169

Borisjuk L, Neuberger T, Schwender J, Heinzel N, Sunderhaus S, Fuchs J, Hay JO, Tschiersch H, Braun HP, Denolf P, et al (2013) Seed architecture shapes embryo metabolism in oilseed rape. Plant Cell **25:** 1625–1640

Brown CS, Huber SC (1987) Photosynthesis, reserve mobilization and enzymes of sucrose metabolism in soybean (Glycine max) cotyledons. Physiol Plant **70:** 537–543

Brown CS, Huber SC (1988) Reserve mobilization and starch formation in soybean (Glycine max) cotyledons in relation to seedling growth. Physiol Plant **72:** 518–524

Buckeridge MS, Dietrich SMC (1996) Mobilization of the raffinose family oligosaccharides and galactomannan in germinating seeds of Sesbania marginata Benth. (Leguminosae-Faboideae). Plant Sci **117:** 33–43

Buckeridge MS, Panegassi V, Dietrich SMC (1995) Storage carbohydrate mobilization in seeds of Dimorphandra mollis Benth. (Leguminosae) following germination. Rev Bras Bot Braz J Bot **18:** 171–175

Buckeridge MS, dos Santos HP, Tiné MAS (2001) Mobilisation of storage cell wall polysaccharides in seeds. Plant Physiol Biochem **38:** 141–156

Buckeridge MS, Aidar MPM, dos Santos HP, Tiné MAS (2004) Acúmulo de reservas. *In* AG Ferreira and F Borghetti,, eds, Germinação do Básico ao Aplicado. Artmed, Porto Alegre, Brazil, pp 31–50

Buitink J, Hemminga MA, Hoekstra FA (2000) Is there a role for oligosaccharides in seed longevity? An assessment of intracellular glass stability. Plant Physiol **122:** 1217–1224

Burley JWA (1961) Carbohydrate translocation in raspberry and soybean. Plant Physiol **36:** 820–824

Canvin DT, Beevers H (1961) Sucrose synthesis from acetate in the germinating castor bean: Kinetics and pathway. J Biol Chem **236:** 988–995

Castro RD, Bradford KJ, Hilhorst HW (2004) Embebição e reativação do metabolismo. *In* AG Ferreira and F Borghetti,, eds, Germinação do Básico ao Aplicado. Artmed, Porto Alegre, Brazil, pp 149–162

Chaudhary J, Patil GB, Sonah H, Deshmukh RK, Vuong TD, Valliyodan B, Nguyen HT (2015) Expanding omics resources for improvement of soybean seed composition traits. Front Plant Sci **6:** 1021

Chen X, Shachar-Hill Y (2012) Insights into metabolic efficiency from flux analysis. J Exp Bot **63:** 2343–2351

Cheung CYM, Williams TCR, Poolman MG, Fell DA, Ratcliffe RG, Sweetlove LJ (2013) A method for accounting for maintenance costs in flux balance analysis improves the prediction of plant cell metabolic phenotypes under stress conditions. Plant J **75:** 1050–1061

Cheung CY, Poolman MG, Fell DA, Ratcliffe RG, Sweetlove LJ (2014) A diel flux balance model captures interactions between light and dark metabolism during day-night cycles in C3 and Crassulacean acid metabolism leaves. Plant Physiol **165:** 917–929

Clemente TE, Cahoon EB (2009) Soybean oil: Genetic approaches for modification of functionality and total content. Plant Physiol **151:** 1030–1040

Colombié S, Nazaret C, Bénard C, Biais B, Mengin V, Solé M, Fouillen L, Dieuaide-Noubhani M, Mazat JP, Beauvoit B, et al (2015) Modelling central metabolic fluxes by constraint-based optimization reveals metabolic reprogramming of developing Solanum lycopersicum (tomato) fruit. Plant J **81:** 24–39

Colombié S, Beauvoit B, Nazaret C, Bénard C, Vercambre G, Le Gall S, Biais B, Cabasson C, Maucourt M, Bernillon S, et al (2017) Respiration climacteric in tomato fruits elucidated by constraint-based modelling. New Phytol **213:** 1726–1739

Crowe JH, Crowe LM, Carpenter JF, Aurell Wistrom C (1987) Stabilization of dry phospholipid bilayers and proteins by sugars. Biochem J **242:** 1–10

Dal'Molin CGDO, Quek LE, Palfreyman RW, Brumbley SM, Nielsen LK (2010) C4GEM, a genome-scale metabolic model to study C4 plant metabolism. Plant Physiol **154:** 1871–1885

Dal'Molin CGDO, Quek LE, Saa PA, Nielsen LK (2015) A multi-tissue genome-scale metabolic modelling framework for the analysis of whole plant systems. Front Plant Sci **6:** 4

Daley DO, Considine MJ, Howell KA, Millar AH, Day DA, Whelan J (2003) Respiratory gene expression in soybean cotyledons during post-germinative development. Plant Mol Biol **51:** 745–755

Day DA, Moore AL, Dry IB, Wiskich JT, Azcon-Bieto J (1988) Regulation of nonphosphorylating electron transport pathways in soybean cotyledon mitochondria and its implications for fat metabolism. Plant Physiol **86:** 1199–1204

Dierking EC, Bilyeu KD (2009) New sources of soybean seed meal and oil composition traits identified through TILLING. BMC Plant Biol **9:** 89

East JW, Nakayama TOM, Parkman S (1972) Changes in stachyose, raffinose, sucrose, and monosaccharides during germination of soybean. Crop Sci **12:** 7–9

Eastmond PJ, Graham IA (2001) Re-examining the role of the glyoxylate cycle in oilseeds. Trends Plant Sci **6:** 72–78

Eastmond PJ, Germain V, Lange PR, Bryce JH, Smith SM, Graham IA (2000) Postgerminative growth and lipid catabolism in oilseeds lacking the glyoxylate cycle. Proc Natl Acad Sci USA **97:** 5669–5674

Eastmond PJ, Astley HM, Parsley K, Aubry S, Williams BP, Menard GN, Craddock CP, Nunes-Nesi A, Fernie AR, Hibberd JM (2015) Arabidopsis uses two gluconeogenic gateways for organic acids to fuel seedling establishment. Nat Commun **6:** 6659

Ebrahim A, Lerman JA, Palsson BO, Hyduke DR (2013) COBRApy: Constraints-based reconstruction and analysis for python. BMC Syst Biol **7:** 74

Empresa Brasileira de Pesquisa Agropecuária (1996) Technical Bulletin: MG/BR-46 (Conquista). Embrapa Soja, Londrina, Brazil

Falk KL, Behal RH, Xiang C, Oliver DJ (1998) Metabolic bypass of the tricarboxylic acid cycle during lipid mobilization in germinating oilseeds: Regulation of NAD^+-dependent isocitrate dehydrogenase versus fumarase. Plant Physiol **117:** 473–481

Fatland BL, Nikolau BJ, Wurtele ES (2005) Reverse genetic characterization of cytosolic acetyl-CoA generation by ATP-citrate lyase in Arabidopsis. Plant Cell **17:** 182–203

Feenstra AD, Alexander LE, Song Z, Korte AR, Yandeau-Nelson MD, Nikolau BJ, Lee YJ (2017) Spatial mapping and profiling of metabolite distributions during germination. Plant Physiol **174:** 2532–2548

Fehr WR, Thorne JC, Hammond EG (1971) Relationship of fatty acid formation and chlorophyll content in soybean seed. Crop Sci **11:** 211–213

Finch-Savage WE, Leubner-Metzger G (2006) Seed dormancy and the control of germination. New Phytol **171:** 501–523

Fontaine JX, Tercé-Laforgue T, Armengaud P, Clément G, Renou JP, Pelletier S, Catterou M, Azzopardi M, Gibon Y, Lea PJ, et al (2012) Characterization of a NADH-dependent glutamate dehydrogenase mutant of Arabidopsis demonstrates the key role of this enzyme in root carbon and nitrogen metabolism. Plant Cell **24:** 4044–4065

Gamborg OL, Finlayson AJ (1969) The amino acid composition of TCA-precipitated proteins and of total residues of plant cells grown in suspension culture. Can J Bot **47:** 1857–1863

Grafahrend-Belau E, Junker A, Eschenröder A, Müller J, Schreiber F, Junker BH (2013) Multiscale metabolic modeling: Dynamic flux balance analysis on a whole-plant scale. Plant Physiol **163:** 637–647

Graham IA (2008) Seed storage oil mobilization. Annu Rev Plant Biol **59:** 115–142

Greenfield H, Southgate DAT (2003) Review of methods of analysis. *In* BA Burlingame, UR Charrondiere, eds, Food Composition Data: Production, Management and Use, Ed 2. FAO, Rome, pp 97–148

Gronwald JW, Jung HG, Litterer LA, Somers DA (2009) Comparison of post-germination mobilization of cell wall polysaccharides and non-cell wall carbohydrates in soybean (Glycine max L.) cotyledons. J Sci Food Agric **89:** 1981–1986

Gurusinghe S, Bradford KJ (2001) Galactosyl-sucrose oligosaccharides and potential longevity of primed seeds. Seed Sci Res **11:** 121–134

Han C, Yin X, He D, Yang P (2013) Analysis of proteome profile in germinating soybean seed, and its comparison with rice showing the styles of reserves mobilization in different crops. PLoS ONE **8:** e56947

Harwood JL (1996) Recent advances in the biosynthesis of plant fatty acids. Biochim Biophys Acta **1301:** 7–56

Hay J, Schwender J (2011) Metabolic network reconstruction and flux variability analysis of storage synthesis in developing oilseed rape (*Brassica napus* L.) embryos. Plant J **67:** 526–541

Hildebrandt TM, Nunes Nesi A, Araújo WL, Braun HP (2015) Amino acid catabolism in plants. Mol Plant **8:** 1563–1579

Holzhütter HG (2004) The principle of flux minimization and its application to estimate stationary fluxes in metabolic networks. Eur J Biochem **271:** 2905–2922

Housley TL, Schrader LE, Miller M, Setter TL (1979) Partitioning of ^{14}C-photosynthate, and long distance translocation of amino acids in preflowering and flowering, nodulated and nonnodulated soybeans. Plant Physiol **64:** 94–98

Hsu SH, Hadley HH, Hymowitz T (1973) Changes in carbohydrate contents of germinating soybean seeds. Crop Sci **13:** 407–410

Joshi AC, Chopra BK, Collins LC, Doctor VM (1973) Distribution of fatty acids during germination of soybean seeds. J Am Oil Chem Soc **50:** 282–283

Junker BH, Klukas C, Schreiber F (2006) VANTED: A system for advanced data analysis and visualization in the context of biological networks. BMC Bioinformatics **7:** 109

Komor E, Orlich G, Weig A, Köckenberger W (1996) Phloem loading—not metaphysical, only complex: Towards a unified model of phloem loading. J Exp Bot **47:** 1155–1164

Koster KL (1991) Glass formation and desiccation tolerance in seeds. Plant Physiol **96:** 302–304

Kruger NJ, Ratcliffe RG (2015) Fluxes through plant metabolic networks: Measurements, predictions, insights and challenges. Biochem J **465:** 27–38

Kuo TM, VanMiddlesworth JF, Wolf WJ (1988) Content of raffinose oligosaccharides and sucrose in various plant seeds. J Agric Food Chem **36:** 32–36

Lalonde S, Tegeder M, Throne-Holst M, Frommer WB, Patrick JW (2003) Phloem loading and unloading of sugars and amino acids. Plant Cell Environ **26:** 37–56

Lalonde S, Wipf D, Frommer WB (2004) Transport mechanisms for organic forms of carbon and nitrogen between source and sink. Annu Rev Plant Biol **55:** 341–372

Laurens LML, Quinn M, Van Wychen S, Templeton DW, Wolfrum EJ (2012) Accurate and reliable quantification of total microalgal fuel potential as fatty acid methyl esters by in situ transesterification. Anal Bioanal Chem **403:** 167–178

LeVan NA, Goggi AS, Mullen R (2008) Improving the reproducibility of soybean standard germination test. Crop Sci **48:** 1933–1940

Libourel IGL, Shachar-Hill Y (2008) Metabolic flux analysis in plants: From intelligent design to rational engineering. Annu Rev Plant Biol **59:** 625–650

Lima JD, Sodek L (2003) N-stress alters aspartate and asparagine levels of xylem sap in soybean. Plant Sci **165:** 649–656

Linka N, Weber AP (2010) Intracellular metabolite transporters in plants. Mol Plant **3:** 21–53

Lisec J, Schauer N, Kopka J, Willmitzer L, Fernie AR (2006) Gas chromatography mass spectrometry-based metabolite profiling in plants. Nat Protoc **1:** 387–396

Lommen A (2009) MetAlign: Interface-driven, versatile metabolomics tool for hyphenated full-scan mass spectrometry data preprocessing. Anal Chem **81:** 3079–3086

Masakapalli SK, Le Lay P, Huddleston JE, Pollock NL, Kruger NJ, Ratcliffe RG (2010) Subcellular flux analysis of central metabolism in a heterotrophic Arabidopsis cell suspension using steady-state stable isotope labeling. Plant Physiol **152:** 602–619

McCleary BV, Matheson NK (1974) α-D-Galactosidase activity and galactomannan and galactosylsucrose oligosaccharide depletion in germinating legume seeds. Phytochemistry **13:** 1747–1757

Mettler IJ, Beevers H (1980) Oxidation of NADH in glyoxysomes by a malate-aspartate shuttle. Plant Physiol **66:** 555–560

Millar AH, Atkin OK, Menz RI, Henry B, Farquhar G, Day DA (1998) Analysis of respiratory chain regulation in roots of soybean seedlings. Plant Physiol **117:** 1083–1093

Millard P, Letisse F, Sokol S, Portais JC (2012) IsoCor: Correcting MS data in isotope labeling experiments. Bioinformatics **28:** 1294–1296

Millhouse J, Wiskich J, Beevers H (1983) Metabolite oxidation and transport in mitochondria of endosperm from germinating castor bean. Aust J Plant Physiol **10:** 167

Mohanty B, Kitazumi A, Cheung CYM, Lakshmanan M, de Los Reyes BG, Jang IC, Lee DY (2016) Identification of candidate network hubs involved in metabolic adjustments of rice under drought stress by integrating transcriptome data and genome-scale metabolic network. Plant Sci **242:** 224–239

Morais ÁA, Silva AL (1996) Composição. *In* ÁA Morais and AL Silva,, eds, Soja: Suas Aplicações. MDSI Editora Médica e Científica, Rio de Janeiro, Brazil, pp 67–77

Moreira TB, Lima JM, Coca GC, Williams TCR (2019) Insights into the spatial and temporal organisation of plant metabolism from network flux analysis. Theor Exp Plant Physiol **31:** 215–226

Muller B, Touraine B (1992) Inhibition of NO_3^- uptake by various phloem-translocated amino acids in soybean seedlings. J Exp Bot **43:** 617–623

Munz E, Rolletschek H, Oeltze-Jafra S, Fuchs J, Guendel A, Neuberger T, Ortleb S, Jakob PM, Borisjuk L (2017) A functional imaging study of germinating oilseed rape seed. New Phytol **216:** 1181–1190

Nielsen N (1996) Soybean seed composition. *In* D Verma and R Shoemaker,, eds, Soybean: Genetics, Molecular Biology and Biotechnology. CAB International, Willingford, United Kingdom, pp 127–163

Nikoloski Z, Perez-Storey R, Sweetlove LJ (2015) Inference and prediction of metabolic network fluxes. Plant Physiol **169:** 1443–1455

Obendorf RL, Zimmerman AD, Ortiz PA, Taylor AG, Schnebly SR (2008) Imbibitional chilling sensitivity and soluble carbohydrate composition of low raffinose, low stachyose soybean seed. Crop Sci **48:** 2396–2403

Ouhida I, Pérez JF, Gasa J (2002) Soybean (Glycine max) cell wall composition and availability to feed enzymes. J Agric Food Chem **50:** 1933–1938

Peterbauer T, Richter A (2001) Biochemistry and physiology of raffinose family oligosaccharides and galactosyl cyclitols in seeds. Seed Sci Res **11:** 185–197

Peterson DM, Housley TL, Schrader LE (1977) Long distance translocation of sucrose, serine, leucine, lysine, and carbon dioxide assimilates. II. Oats. Plant Physiol **59:** 221–224

Pfau T, Christian N, Masakapalli SK, Sweetlove LJ, Poolman MG, Ebenhöh O (2018) The intertwined metabolism during symbiotic nitrogen fixation elucidated by metabolic modelling. Sci Rep **8:** 12504

Poolman MG, Miguet L, Sweetlove LJ, Fell DA (2009) A genome-scale metabolic model of Arabidopsis and some of its properties. Plant Physiol **151:** 1570–1581

Pracharoenwattana I, Cornah JE, Smith SM (2005) Arabidopsis peroxisomal citrate synthase is required for fatty acid respiration and seed germination. Plant Cell **17:** 2037–2048

Praxedes SC, DaMatta FM, Loureiro ME, Ferrão MA, Cordeiro AT (2006) Effects of long-term soil drought on photosynthesis and carbohydrate metabolism in mature robusta coffee (Coffea canephora Pierre var. kouillou) leaves. Environ Exp Bot **56:** 263–273

Raymond P, Spiteri A, Dieuaide M, Gerhardt B, Pradet A (1992) Peroxisomal β-oxidation of fatty acids and citrate formation by a particulate fraction from early germinating sunflower seeds. Plant Physiol Biochem **30:** 153–161

Robinson SA, Slade AP, Fox GG, Phillips R, Ratcliffe RG, Stewart GR (1991) The role of glutamate dehydrogenase in plant nitrogen metabolism. Plant Physiol **95:** 509–516

Rohn H, Hartmann A, Junker A, Junker BH, Schreiber F (2012) FluxMap: A VANTED add-on for the visual exploration of flux distributions in biological networks. BMC Syst Biol **6:** 33

Rolletschek H, Grafahrend-Belau E, Munz E, Radchuk V, Kartäusch R, Tschiersch H, Melkus G, Schreiber F, Jakob PM, Borisjuk L (2015) Metabolic architecture of the cereal grain and its relevance to maximize carbon use efficiency. Plant Physiol **169:** 1698–1713

Rossi MT, Kalde M, Srisakvarakul C, Kruger NJ, Ratcliffe RG (2017) Cell-type specific metabolic flux analysis: A challenge for metabolic phenotyping and a potential solution in plants. Metabolites **7:** E59

Rotundo JL, Westgate ME (2009) Meta-analysis of environmental effects on soybean seed composition. Field Crops Res **110:** 147–156

Saha R, Suthers PF, Maranas CD (2011) Zea mays iRS1563: A comprehensive genome-scale metabolic reconstruction of maize metabolism. PLoS ONE **6:** e21784

Salon C, Raymond P, Pradet A (1988) Quantification of carbon fluxes through the tricarboxylic acid cycle in early germinating lettuce embryos. J Biol Chem **263:** 12278–12287

Servaites JC, Schrader LE, Jung DM (1979) Energy-dependent loading of amino acids and sucrose into the phloem of soybean. Plant Physiol **64:** 546–550

Shamimuzzaman M, Vodkin L (2014) Transcription factors and glyoxylate cycle genes prominent in the transition of soybean cotyledons to the first functional leaves of the seedling. Funct Integr Genomics **14:** 683–696

Shaw R, Cheung CYM (2018) A dynamic multi-tissue flux balance model captures carbon and nitrogen metabolism and optimal resource partitioning during Arabidopsis growth. Front Plant Sci **9:** 884

Silva DJ, Venegas VHA, Ruiz HA, Sant'Anna R (2003) Translocação e redistribuição de enxofre em plantas de milho e de soja. Pesqui Agropecu Bras **38:** 715–721

Simeonidis E, Price ND (2015) Genome-scale modeling for metabolic engineering. J Ind Microbiol Biotechnol **42:** 327–338

Spears JF, Tekrony DM, Egli DB (1997) Temperature during seed filling and soybean seed germination and vigour. Seed Sci Technol **25:** 233–244

Stepansky A, Galili G (2003) Synthesis of the Arabidopsis bifunctional lysine-ketoglutarate reductase/saccharopine dehydrogenase enzyme of lysine catabolism is concertedly regulated by metabolic and stress-associated signals. Plant Physiol **133:** 1407–1415

Tan-Wilson AL, Wilson KA (2012) Mobilization of seed protein reserves. Physiol Plant **145:** 140–153

Thiele I, Palsson BO (2010) A protocol for generating a high-quality genome-scale metabolic reconstruction. Nat Protoc **5:** 93–121

Thorne JH (1982) Characterization of the active sucrose transport system of immature soybean embryos. Plant Physiol **70:** 953–958

Turano FJ, Dashner R, Upadhyaya A, Caldwell CR (1996) Purification of mitochondrial glutamate dehydrogenase from dark-grown soybean seedlings. Plant Physiol **112:** 1357–1364

Vieira CR, Cabral LC, De Paula ACO (1999) Proximate composition and amino acid, fatty acid and mineral contents of six soybean cultivars for human consumption. Pesqui Agropecu Bras **34:** 1277–1283

Vitor SC, do Amarante L, Sodek L (2018) Are phloem-derived amino acids the origin of the elevated malate concentration in the xylem sap following mineral N starvation in soybean? Planta **248:** 437–449

Webster BD, Leopold AC (1977) The ultrastructure of dry and imbibed cotyledons of soybean. Am J Bot **64:** 1286–1293

Weise A, Barker L, Kühn C, Lalonde S, Buschmann H, Frommer WB, Ward JM (2000) A new subfamily of sucrose transporters, SUT4, with low affinity/high capacity localized in enucleate sieve elements of plants. Plant Cell **12:** 1345–1355

Weitbrecht K, Müller K, Leubner-Metzger G (2011) First off the mark: Early seed germination. J Exp Bot **62:** 3289–3309

Williams TCR, Poolman MG, Howden AJM, Schwarzländer M, Fell DA, Ratcliffe RG, Sweetlove LJ (2010) A genome-scale metabolic model accurately predicts fluxes in central carbon metabolism under stress conditions. Plant Physiol **154:** 311–323

Yazdi-Samadi B, Rinne RW, Seif RD (1977) Components of developing soybean seeds: Oil, protein, sugars, starch, organic acids, and amino acids. Agron J **69:** 481–486

Yuan H, Cheung CYM, Hilbers PA, van Riel NA (2016a) Flux balance analysis of plant metabolism: The effect of biomass composition and model structure on model predictions. Front Plant Sci **7:** 537

Yuan H, Cheung CYM, Poolman MG, Hilbers PAJ, van Riel NAW (2016b) A genome-scale metabolic network reconstruction of tomato (Solanum lycopersicum L.) and its application to photorespiratory metabolism. Plant J **85:** 289–304

Ziegler P (1995) Carbohydrate degradation during germination. *In* J Kigel, G Galili, eds, Seed Development and Germination. Marcel Dekker, New York, pp 447–474